



Universidad de Valladolid

FACULTAD DE CIENCIAS

TRABAJO FIN DE GRADO

Grado en Química

**COMPOSITE FERROELECTRICS FOR RECYCLABLE ENERGY
HARVESTING AND SENSING APPLICATIONS – PLASTIC
CRYSTAL MATRIX AND CERAMIC PEROVSKITE PARTICLES**

Autora: Lucía Pedraza de Frutos

Tutores: Héctor Barbero San Juan y Julian Walker

Junio, 2024

Acknowledgements

I would like to express my gratitude to my NTNU supervisor, Julian Walker, for his assistance and guidance throughout this year, in the experimental and theoretical work in Norway. I also want to thank my supervisor in Valladolid, Héctor Barbero San Juan, for his help whenever I needed it. It was a fantastic experience to learn from both of you.

I am thankful to my family, my parents, my sister and the friends that the Chemistry Degree has given me, who supported me from afar, as well as Víctor for making this project possible in many ways. Additionally, I am grateful to my new friends who have appeared in my life and supported me throughout this year: Charbel, Cippora, Judit and Luis.

Contents

1	Introduction	1
1.1	Background and motivation	1
1.2	Theory and Literature	2
1.2.1	Ferroelectric Materials	2
1.2.2	BaTiO ₃	5
1.2.3	Plastic Crystals	7
1.2.4	Ferroelectric Composites	8
2	Aim and scope of the work	10
3	Experimental	11
3.1	Chemicals	11
3.2	Procedures	11
3.2.1	TMA FBC Synthesis	11
3.2.2	Mixing of Compounds	13
3.2.3	Hot Pressing	14
3.2.4	Gold Sputter Coating	15
3.2.5	X-Ray Diffraction (XRD)	15
3.2.6	Scanning Electron Microscopy (SEM)	15
3.2.7	Pycnometry	16
3.2.8	Particle-Size Distribution (PSD) Analysis	16
3.2.9	Ferroelectric measurements	16
3.2.10	Dielectric measurements	17
4	Results	18
4.1	Tetramethylammonium bromotrichloroferrate(III) (TMA FBC)	18
4.1.1	Structural Characterization	18
4.1.2	Surface Characterization	19
4.2	BaTiO ₃	20
4.2.1	Structural Characterization	20
4.2.2	Density Characterization	21
4.2.3	Particle-Size Distribution Characterization	21
4.2.4	Surface Characterization	21
4.3	Composite	22
4.3.1	Structural Characterization	22
4.3.2	Density Characterization	24
4.3.3	Surface Characterization	24
4.3.4	High Voltage Ferroelectric Properties Characterization	28
4.3.5	Dielectric Properties Characterization	32
5	Discussion	34
5.1	TMA FBC Synthesis and Characterization.	34
5.2	Ceramic Characterization.	34
5.3	Composites Characterization.	35

6 Conclusions	38
References	39
List of Figures	43
List of Tables	43

List of Acronyms

C Curie Constant

CAS Chemical Abstracts Service

E Electric Field

Ec Coercive Electric Field

LASER Light Amplification by Stimulated Emission of Radiation

P Polarization

Ps Saturation Polarization

PSD Particle-Size Distribution

Pr Remnant Polarization

PVDF Polyvinylidene Fluoride

PZT Lead Zirconate Titanate

rpm revolutions per minute

SEM Scanning Electron Microscopy

T Temperature

Tc Curie Temperature

TMA FBC Tetramethylammonium bromotrichloroferrate(III)

UN United Nations

XRD X-Ray Diffraction

Abstract

Ferroelectric materials are critical components in nearly all our wireless communication technologies, used in applications such as sensors or antennas. However, state-of-the-art materials are limited to metal oxides or polymers (Polyvinylidene Fluoride (PVDF)) and are not recyclable. This work involved obtaining a composite ferroelectric from a plastic crystal (TMA FBC) matrix, synthesized in the laboratory using different evaporation and condensation methods, together with perovskite BaTiO₃ particles. For this process, pressed pellets were formed at high temperatures using fixed compositions of 10, 30 and 50 % in volume for the BaTiO₃. The characterization of the properties of both, the precursor materials and the final composites was carried out using analytical methods including X-ray diffraction, SEM imaging, high-voltage ferroelectric testing and dielectric impedance measurements. It was observed that the plastic crystal synthesis was challenging to obtain one single phase, as it required two crystallization processes within the process. The main interest lies in studying how the ferroelectric and dielectric properties of this new material change as a function of the composition. The results showed that the materials exhibit adequate ferroelectric behaviour, with strain values and ferroelectric and dielectric parameters changing as the composition varied, improving when the ceramic presence was higher. Tests revealed that the pellet containing 30 % of BaTiO₃ in volume, had the lowest dielectric permittivity (ϵ') and dielectric loss ($\tan(\delta)$), so it may be interesting depending on the desired applications.

Abstract

Los materiales ferroeléctricos son componentes muy extendidos en las tecnologías de comunicación inalámbricas, utilizados en aplicaciones como sensores o antenas. Sin embargo, los materiales de última generación se limitan a compuestos como óxidos metálicos o polímeros (PVDF) y no son reciclables. Este trabajo implicó la obtención de un material ferroeléctrico compuesto a partir de una matriz cristalina plástica (TMA FBC), sintetizada en el laboratorio utilizando diferentes métodos de evaporación y condensación, junto con partículas de la perovskita BaTiO₃. Posteriormente, se formaron pellets prensados a altas temperaturas utilizando composiciones fijas de 10, 30 y 50 % en volumen para el BaTiO₃. La caracterización de las propiedades, tanto de los materiales precursores, como de los compuestos finales se llevó a cabo utilizando métodos analíticos entre los que se incluyen difracción de rayos X, imágenes de SEM, pruebas ferroeléctricas de alto voltaje y mediciones de impedancia dieléctrica. Se observó que la síntesis de cristales plásticos era desafiante para obtener una sola fase, ya que el proceso requirió dos procesos de cristalización. El principal interés radica en estudiar cómo cambian las propiedades ferroeléctricas y dieléctricas de este nuevo material, en función de su composición. Los resultados mostraron que los materiales presentan un comportamiento ferroeléctrico adecuado, con valores de deformación y parámetros ferroeléctricos y dieléctricos cambiantes a medida que varía la composición, mejorando cuando la presencia de la cerámica es mayor. Las pruebas revelaron que el pellet con 30 % de BaTiO₃ en volumen, tiene la permitividad dieléctrica (ϵ') y la pérdida dieléctrica ($\tan(\delta)$) más bajas, por lo que puede ser interesante en función de las aplicaciones deseadas.

1 Introduction

1.1 Background and motivation

The field of ferroelectric materials has had a significant impact on today's technological advances [1]. This is because they are part of applications that include everything from cutting-edge aeronautical technology to products that are consumed daily in the world such as speakers and radio frequency antenna. Some examples of ferroelectric materials are sensors, transducers, igniters, and vibration generators in different fields such as piezoelectric or optical [2]. For most of these applications, it is important to study the properties of the materials, to understand their relationship with their structure. Some of the studied parameters are the characteristically high dielectric constant, remnant polarization and piezoelectric coefficients [3]. It is necessary to know these properties of the material to understand both its molecular structure and its polarization mechanism.

A particular example of ferroelectric materials, specifically ferroelectric ceramics, is the perovskite-type compositions. There is a diverse range of these compositions, so they can be widely engineered. They are highlighted because of their excellent piezoelectric and dielectric properties. In the last 75 years, a large number of ceramics of this type have been studied, which includes BaTiO₃ [3].

Currently, new examples of ferroelectric materials are emerging and being studied, in search of materials with better properties, lead-free and sustainable. Some examples of new suitable ferroelectric materials are ionic plastic crystals. These specific have moderate polarization and piezoelectric coefficients [4], that, in addition to their plasticity properties, can lead to potentially improved materials in the field.

Taking this into account, as observed in other studies [5], it could be interesting to study the fabrication of new materials based on the combination of the formerly presented elements. Designing it with a matrix of plastic crystals and perovskite ceramic particles and investigating their resulting properties.

Furthermore, a remarkable property of plastic crystals that, in this case, can be used as an advantage, is their solubility. This could open up the possibility of material recovery and recycling of molecular components made from this composite. The result could combine the ferroelectric properties of both materials and may lead to a new sustainable compound, following the United Nations (UN) sustainable development goal number 12, which refers to responsible consumption and production patterns [6].

1.2 Theory and Literature

1.2.1 Ferroelectric Materials

Ferroelectric materials belong to a class of polar dielectric materials, characterized by their ability to change the direction of their spontaneous polarization under an electric field [1]. These compounds are part of a class of insulating materials known as dielectrics. These can maintain a dielectric polarization under an electric field. Among the 32 point groups in crystal systems, 21 are non-centrosymmetric [7], so they do not have a symmetric centre in their crystal structure. Due to this lack of symmetry, they exhibit piezoelectric behaviour. Piezoelectricity is the ability of some materials to generate an electrical charge or polarize in response to an applied mechanical stress and it is measured by the piezoelectric coefficient or constant (d_{33} [=] C/N). Another important parameter to take into consideration is the electromechanical coupling factor, k_{ij} . This factor helps us understand the relationship between mechanical and electrical energy, and the efficacy with which the material converts one type of energy into the other and vice versa. Some of the non-centrosymmetric crystals also exhibit an axis of symmetry, making them polar. These crystals have also pyroelectric properties, in addition to being piezoelectric. Pyroelectricity refers to the separation of charges with temperature changes [8].

The relation between the dielectric, piezoelectric, pyroelectric and ferroelectric materials is observed in Figure 1. Every ferroelectric material presents also pyroelectric, piezoelectric and dielectric behaviour.

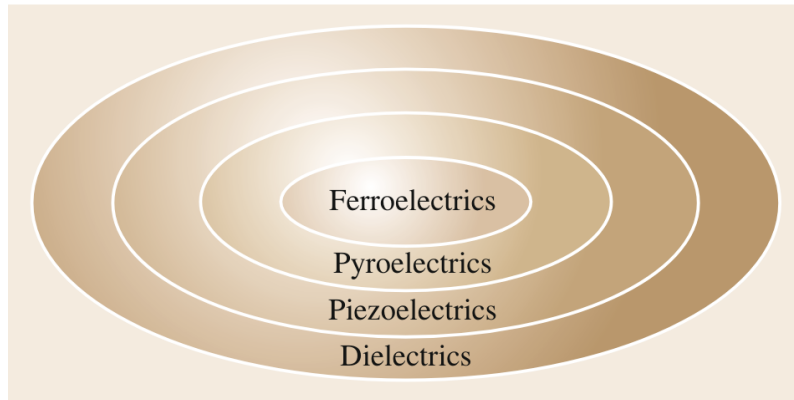


Figure 1: Venn diagram with the relations between electric properties of materials [8].

Ferroelectric materials exhibit features such as domain structures, hysteresis loops and a Curie temperature. The domains are uniform polarization regions that are separated by domain walls. When a strong electric field is applied, the domains can align in a single direction, potentially leading to domain switching [9]. The spontaneous polarization of these materials can be reversed by a strong electric field, leading to a hysteresis loop and dependencies on the material's history and the applied field [7]. In the hysteresis loops, as the electric field strength increases, the domains align in the positive direction, leading to a fast increase in polarization. The Saturation Polarization (P_s) is reached at high field levels, but a Remnant Polarization (P_r) endures when the external field is removed. To reduce the polarization to zero an external field, called Coercive Electric Field (E_c), is needed [9]. The complete hysteresis loop is represented in Figure 2.

by the USSR and MIT revealed that the high dielectric constant of BaTiO_3 was due to its ferroelectric properties. Furthermore, in 1945 was found that external electric fields could orient the domains within the grains of this ceramic, transforming it into a material with ferroelectric and piezoelectric properties. This process, known as "poling", allowed inert ceramics to be converted into electromechanically active materials with a variety of industrial and commercial applications. It was a surprising discovery because previously it was believed that ceramics could not exhibit piezoelectric activity due to their randomly oriented crystals [9].

The use of ferroelectrics is vast and covers a wide range of applications, including non-volatile computer memory storage, high-permittivity capacitors, piezoelectric sensors and actuators, pyroelectric detectors, electro-optical devices, non-linear optics, and acousto-optic interactions. Therefore, ferroelectric materials have a promising future [8]. These materials are also an integral part of multi-billion-dollar industries [1], ranging from crystals to polymers and even liquid crystals [8]. For instance, perovskite-type ceramic ferroelectric materials, like BaTiO_3 , have been the foundation of several industries, based on capacitor applications, since their discovery in the early 1940s [3]. Ferroelectric materials, as has been seen, have a long history in terms of their applications, therefore contemporary research seeks to meet a series of objectives that take sustainability and affordability into account. Some specific objectives are included in the scheme in Figure 3.

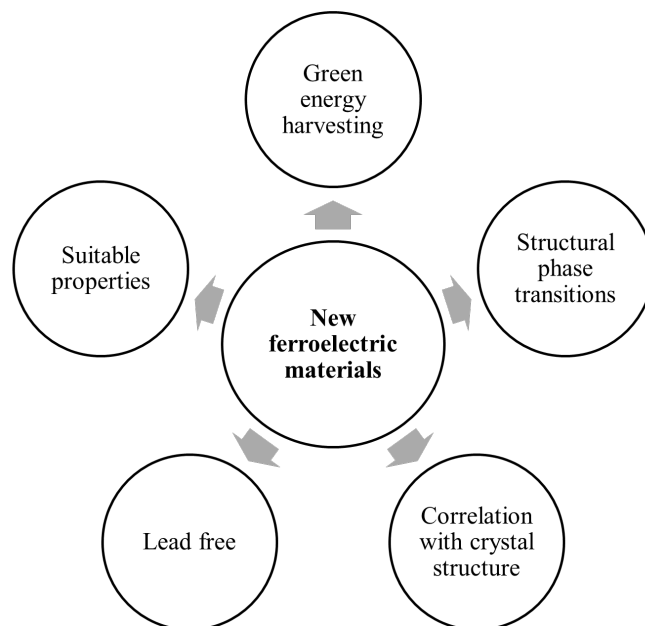


Figure 3: Scheme on the relevant aspects of new ferroelectric materials.

Due to their ability to modify their micro-geometry, ferroelectric compounds are also known as "smart" materials. The resulting variations in their physical properties can be achieved by combining different types of composites, such as a ceramic and a polymer, a single crystal and a ceramic, or a single crystal and a polymer. The different compositions and components allow for parameter tuning or properties that are not specific to the separate components. The properties variation can be fundamental for many practical

transducer applications. Additionally, the properties of these materials largely depend on factors such as manufacturing and polarization methods, temperature history, mechanical stress history, and microstructure [1].

In this study, we will explore the properties of a ferroelectric material with a specific composition obtained by combining a plastic crystal and a ceramic. This ceramic is lead-free and due to the plastic crystal properties, the new material could lead to applications in green energy harvesting.

1.2.2 BaTiO₃

BaTiO₃ was the first perovskite ceramic to be discovered during the II World War, and it is known as a clear example of ferroelectric material [11]. Structurally, the perovskite compounds have a general formula of ABO_3 , where, in this case, the Ba^{2+} atoms are located in the A site at the corners of the face-centred cubic unit cell, as shown in Figure 4, while Ti^{4+} occupies the B site in the centre of the cell. The O^{2-} anions are located at the face centres of the unit cell and constitute an octahedron.

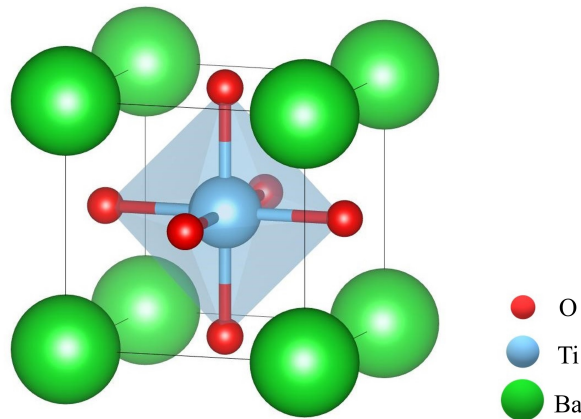


Figure 4: Structural model of the unit cell of the face-centred cubic system BaTiO₃.

The ferroelectric properties of BaTiO₃ are due to its polymorphic, displacive phase transition from a high-temperature prototype phase (often centrosymmetric) to a non-centrosymmetric ferroelectric phase. Below this temperature, the material undergoes two additional polymorphic phase transitions to orthorhombic and rhombohedral phases, that are also non-centrosymmetric and thus ferroelectric [12]. The Figure 5 shows the different phases and their corresponding relative dielectric constant (ϵ_r), as a function of the temperature. The spontaneous polarization at its Curie temperature (120 °C) and tetragonal phase, happens along one of the directions of the cubic structure labelled as [001] [9].

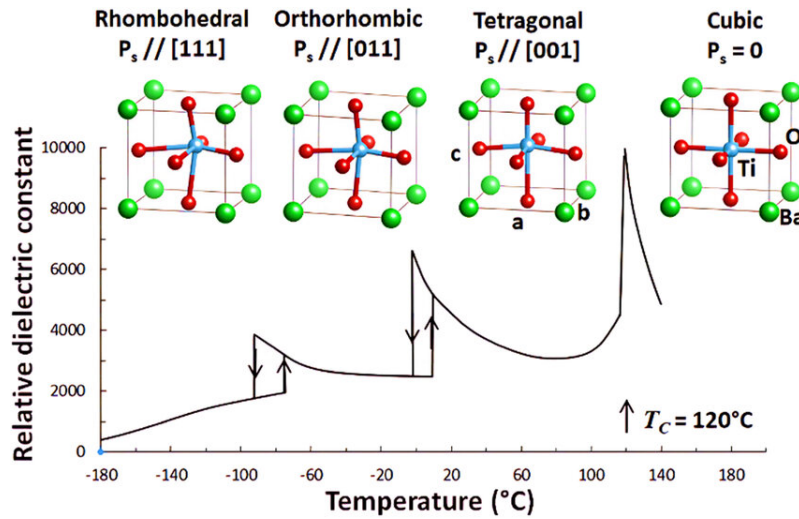


Figure 5: Temperature dependence of the relative dielectric constant of pure BaTiO₃ [13].

Engineered synthesis routes can obtain fine domain structures and so, improve the piezoelectric and dielectric properties of the material. As a ferroelectric compound, the microstructure of this perovskite affects its electrical properties. Some parameters, that can be optimized in the synthesis and use of the ceramic, are its grain size and domain configuration. The grain size can influence the dielectric and piezoelectric properties, enhancing at the same time, the domain wall density. In this case, with the increasing of the grain size of this ceramic, the domain size is increased but it happens the opposite for its piezoelectricity. It has been studied that the optimum size is between 1 μm and 2.3 μm . For instance, a grain size between 10 nm and 100 nm can cause a non-ferroelectric state, at room temperature [9].

The chemical compound BaTiO₃ is known for its relatively high stability components, which facilitate sintering and maintain good chemical stoichiometry [3]. However, pure unmodified BaTiO₃ has a low piezoelectric constant (191 pC/N) which can be improved by modifying its structural characteristics or combining it with special additives. For example by substituting the A and B sites in the perovskite structure, to modify and improve their basic electrical properties [11].

BaTiO₃ was used firstly as a piezoelectric transducer, in sonar detection or photograph needles [11]. Nowadays, its applications have changed to high dielectric constant capacitors of different types. This is because their Curie temperature is relatively lower than 120 °C, which limits their use as high-power transducers. It also has a low electromechanical coupling factor compared to PZT (another used piezoelectric ceramic), which can limitate its performance [3]. BaTiO₃, in particular, has been a dominant material in the field of ferroelectric ceramic and has played an important role in various applications due to its ferroelectric nature and specific application areas, such as switches, sensors, motor starters, and controllers. Including also medical, non-destructive ultrasound, underwater testing and sonar, and the production of ferroelectric random access memory (FeRAM), a type of non-volatile memory, faster and more energy efficient than traditional flash memory [3].

1.2.3 Plastic Crystals

Plastic crystals are part of a class of compounds called crystalline dynamic solids [14]. These unique supramolecular materials have a structure based on a matrix of ions or neutral molecules that form a crystal lattice [4]. The plastic crystals combine local structural disorder with long-range crystallographic order. The long-range structure can determine properties like piezoelectricity and ferroelectricity. On the other hand, the local structural disorder is produced by molecular orientation freedom, causing increases in entropy and ionic conductivity. The rotation of molecules is not linearly influenced by the temperature. However, the molecular components can show orientational freedom when transitioning from a solid to a mesophase, at a consistent temperature. This shift leads the material to a mesophase state before melting [15]. This mesophase state refers to the intermediate state that exhibits both crystalline and amorphous (glass transition) characteristics. It is measured by a translational periodicity degree, resulting in narrow peaks in X-ray diffraction structure [16].

The mesophase transition of plastic crystals allows them to flow and plastically deform at temperatures above their melting point, due to the weak intermolecular bonds and the increasing orientational freedom [17]. They can undergo permanent deformation without fracturing due to the large number of slip planes in their highly symmetrical crystals, making them malleable and suitable for making films [14]. As shown with their properties, the plastic crystals represent a new group of ferroelectric crystals that have different properties than other molecular ferroelectric crystals used in the past [18]. Taking into account these physical and electrical properties, there has been considerable interest in developing research about their potential applications in recent years [14].

TMA FBC

Tetramethylammonium bromotrichloroferrate(III) ($[\text{N}(\text{CH}_3)_4][\text{FeBrCl}_3]$) is a specific type of plastic crystal that has been studied for its properties [17], which combines low dielectric constants, strong piezoelectric coefficients, and ferroelectricity at room temperature [4]. One drawback of the material is that it also exhibits leakage currents that contribute to the change in behaviour, at higher frequencies. Its structure is non-centrosymmetric orthorhombic (with a phase named "Amm2", Figure 6) at room temperature. It has three temperature-dependent polymorphs between 0 and 110 °C. The material can be synthesized using aqueous solvents and temperatures not exceeding 140 °C [17]. The structure of plastic crystals, such as $[\text{N}(\text{CH}_3)_4][\text{FeBrCl}_3]$, can be analysed using different techniques, including X-ray diffraction, Raman spectroscopy, and infrared spectroscopy [4].

Furthermore, due to their constitution of ions, tetramethylammonium cation and bromotrichloroferrate(III) anion, this plastic crystal was found to be water-soluble. This factor could be interesting for the recyclability of molecular components and recovery of any material it can be part of [15].

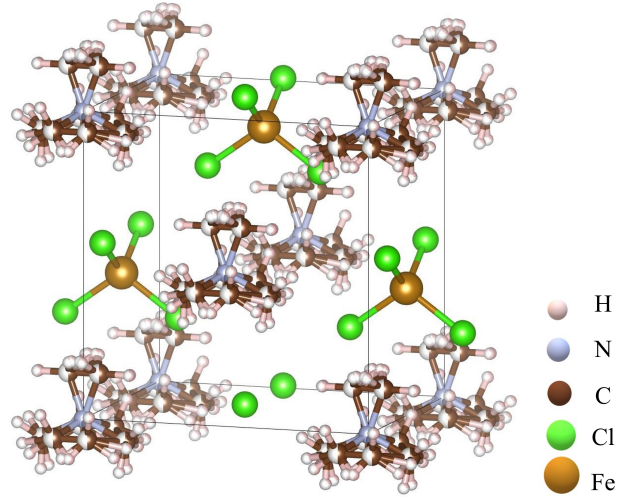


Figure 6: Structural model of the unit cell of orthorhombic TMA FBC.

1.2.4 Ferroelectric Composites

This work is based on other studies of materials that have been synthesized by combining different classes of compounds, to obtain supramolecular composites with interesting ferroelectric properties. The aim of creating this hybrid material is to reach a convenient solution for improving both, mechanical and electrical properties [5].

Many studies are being carried out on ferroelectric compounds, that combine different materials to explore new applications, such as electrical, optoelectronic, energy harvesting or biomedical devices. An example of these combinations is ceramic-polymer composites. According to the mixing ratio of polymer matrix with ceramic filler, optimal properties can be obtained for different purposes, as represented in Figure 7. In the resulting mixtures, factors, such as a high dielectric constant and low dielectric loss of the polymer matrix, with a uniform distribution of the ceramic as a filler, are combined [19].

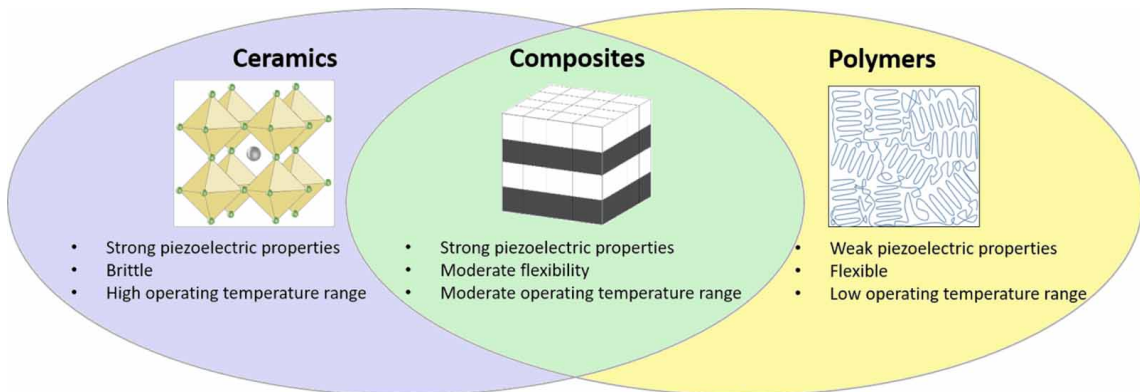


Figure 7: Scheme of the combined properties of a ceramic and a polymer composite [11].

In the past, polymers such as PVDF and its copolymers have been used due to their dielectric and ferroelectric properties [19]. These polymer piezoelectrics are also flexible

and lightweight. On the other hand, ceramic piezoelectric materials show stronger piezoelectric performance, but they are rigid and brittle [11]. Incorporating perovskite-based ceramics like BaTiO_3 , can also help to avoid problems of high dielectric loss and low dielectric breakdown strength of the polymer materials [19]. In conclusion, composite materials are a potential innovation that combines the advantages of ceramics and polymers, offering customizable properties through structural and compositional modifications [11].

With this basis in mind, this work is going to focus on the creation of a ferroelectric composite, by using a matrix of plastic crystal, instead of a polymer. The electrical properties of the original material will be enhanced by the dispersion of variable proportions of BaTiO_3 particles, as seen in other composite materials.

2 Aim and scope of the work

The final aim of this project is to synthesise, for the first time, a new composite based on a plastic crystal (TMA FBC) and BaTiO_3 , and to study the properties as a function of volume percentage of the ceramic particles. In order to do so, it will be necessary to obtain the appropriate precursors, synthesising the TMA FBC, and characterising its structure, as well as characterising the ceramic that will be used. Through this process, we will gain a thorough understanding of the potential properties and behaviours, and the adequacy of the precursors for the main purpose.

The main objectives can be decomposed into primary and secondary ones. Our primary objective is to understand the change of functional electrical properties, such as the variation in the polarization, strain and permittivity, as a function of the composition, expressed as a volume percentage of BaTiO_3 , in the composite. The composites obtained will be analysed using various techniques and instruments, such as X-ray diffraction XRD and SEM, for structural and surface analysis.

The secondary objective is to develop an appropriate synthesis method for this unique material. In order to achieve this goal, we will use a singular property of TMA FBC, which is its deformability, in its mesophase. A hot pressing method will be used to heat and press the mix of TMA FBC with BaTiO_3 , obtaining a dense composite in the form of bulk pellets. These pellets are based on the mixture of the components, with a fixed composition of 10, 30 and 50 % of BaTiO_3 in volume. Including as an objective, the identification of any other key challenges observed with these materials, during their study.

3 Experimental

3.1 Chemicals

Among the chemicals used, the precursors of the plastic crystal (TMA FBC) are: tetramethylammonium bromide ($\text{N}(\text{CH}_3)_4\text{Br}$) and iron (III) chloride hexa-hydrated ($\text{FeCl}_3 \cdot 6\text{H}_2\text{O}$). For the ceramic, a commercial (BaTiO_3) powder is used. The relevant information, about the chemical compounds and solvent used, is gathered in Table 1.

Table 1: Commercial compounds with their Chemical Abstracts Service (CAS) used for the experimental procedures.

Compound	CAS	Use	Purity	Company
$\text{FeCl}_3 \cdot 6\text{H}_2\text{O}$	10025-77-1	Precursor of TMA FBC	$\geq 99\%$	Sigma-Aldrich
$\text{N}(\text{CH}_3)_4\text{Br}$	64-20-0	Precursor of TMA FBC	98 %	Sigma-Aldrich
BaTiO_3	120-47-27-7	Perovskite ceramic	99 %	Sigma-Aldrich
Ethanol	64-17-5	Solvent	100 % (absolute)	VMR chemicals

3.2 Procedures

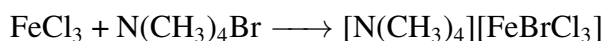
3.2.1 TMA FBC Synthesis

After weighing the appropriate amount of the precursors in the form of powder (mass values obtained using a mix sheet, captured in Table 2), they are dissolved separately in distilled water. They are stirred at 200 revolutions per minute (rpm) and room temperature for approximately 10 minutes until they are completely dissolved.

Table 2: Stoichiometric relations and compounds used for the synthesis of 20 g of TMA FBC.

Compound	Molar Mass	Molar ratio	Mass needed
$\text{FeCl}_3 \cdot 6\text{H}_2\text{O}$	270.30 g/mol	1	17.44 g
$\text{N}(\text{CH}_3)_4\text{Br}$	154.05 g/mol	1	9.94 g

Subsequently, the solutions are combined in a crystallizer, and stirred for 10 minutes, at room temperature and 200 rpm. Then, it is left to crystallize at room temperature. The crystals precipitate slowly through the evaporation of water. This process takes around 2 days to complete. The reaction with stoichiometry 1:1 that takes place is:



Afterwards, it is necessary to filter the crystals, to separate them from the solution that has not precipitated. For this process, a vacuum filtration system is used. This instrumentation uses a filtering flask, and a funnel with a filtering paper. The flask is connected to a vacuum pump, so the humidity of the crystals is sucked into the flask and the crystals remain on the filtering paper completely dried (Figure 8).



Figure 8: Photograph of a filtering flask, funnel, filtering paper and the dark red crystalline product.

Following these steps, the crystals are dried in a vacuum oven at 60 °C, for 5 hours. Then, it is essential to recrystallize the crystals formed, to eliminate impurities or precursors that have not reacted. Around 150 ml of ethanol is used in this procedure, to redissolve the compound in a round flask, suitable for a rotary evaporator. This instrument is used at 70 °C without the distilling or vacuum mode, just letting the ethanol dissolve the crystals in the water bath, at that temperature (Figure 9).

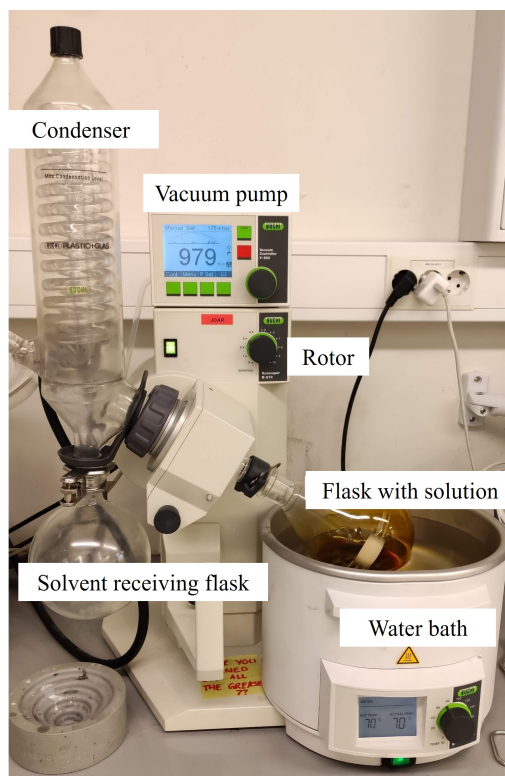


Figure 9: Photograph of the rotary evaporator used for the recrystallization, with its parts labelled.

Once all the crystals have been dissolved, the flask is rapidly placed in a freezer at $-18\text{ }^{\circ}\text{C}$. A fast temperature transition is necessary to obtain crystals of minimal size. Finally, in order to dry the pure crystals (Figure 10), a vacuum oven is used at $60\text{ }^{\circ}\text{C}$, for 5 hours.



Figure 10: Dark red TMA FBC crystals before (left) and after (right) the recrystallization process.

3.2.2 Mixing of Compounds

In order to proceed with the fabrication of the pressed pellets, firstly, the mixture of the TMA FBC and BaTiO_3 is needed. For this purpose, a mortar and a pestle are used, as seen in Figure 11. The TMA FBC synthesized has small crystals, due to the fast transition of temperatures, after the recrystallization while the commercial BaTiO_3 has also small particles, making the mix look homogeneous.



Figure 11: Mix of the composites in powder form, in a mortar and pestle.

As the aim is to compare the properties of the resulting composite, depending on the ratio of the precursors, the compounds are mixed with different proportions, classified by the percentage of the BaTiO_3 volume, as captured in Table 3. The densities used for

the calculus are 1.48 g/ml for the TMA FBC [15] and 6.14 g/ml for the BaTiO₃ (value obtained in section 4.2.2).

Table 3: Amount of mass needed of the precursors to obtain the different composites.

Label	% in volume of ceramic	TMA FBC (g)	BaTiO ₃ (g)
10	10 %	1.73	0.80
30	30 %	1.35	2.39
50	50 %	0.96	3.98

3.2.3 Hot Pressing

Regarding this procedure, a hot press with two flat heating plates is used. For this instrument, we needed two steel plates to contain the sample and two films of aluminium foil inside, used as lubricant and protector of the composite (as shown in Figure 12). The temperature is set at 200 °C in both plates, and the pressing takes 15 minutes for each pellet.

In this process there is nothing that restricts the flow of the samples in the horizontal direction during pressing, so as the mixture deforms with pressure and temperature the samples spread out (Figure 13). After the process, the pellet is divided into 4 pieces of the same size, for different characterization methods. This procedure is repeated for the pellets with different compositions (Figure 13). Additionally, for further characterization analysis, a pellet made of 100 % TMA FBC is pressed at 250 °C.

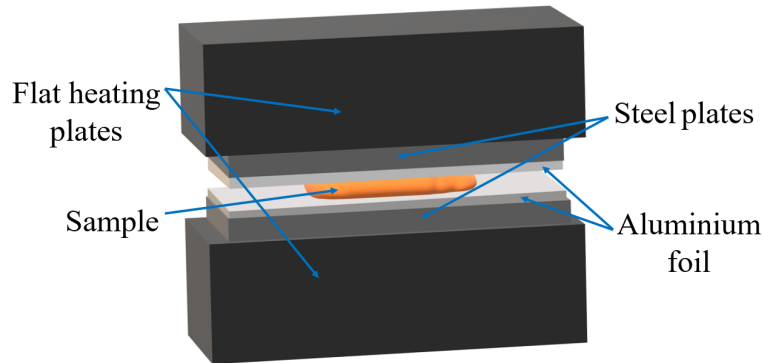


Figure 12: Hot Press Model used for obtaining the composite pellets.

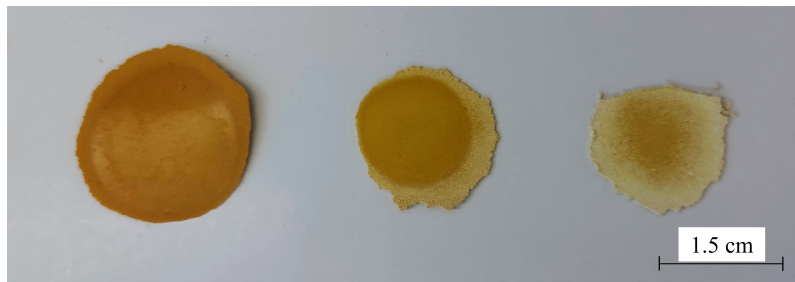


Figure 13: Pellets of 10, 30 and 50 % of BaTiO₃ in volume from left to right, obtained with the flat heating hot press (diameters around 2-3 cm).

3.2.4 Gold Sputter Coating

This procedure is necessary for the electrical characterization of the pellets obtained in 3.2.3.

With an Edwards Sputter Coater S150B, a thin layer of gold metal is applied to the material (Figure 14), pumping a gold surface with Argon ions. This process is done on the surface of both sides of the pellets, so they will be used as electrodes.

The procedure was carried out for 3 minutes, on each side of the pellet, with a current of 10 mA and using a vacuum system to eliminate atmospheric air. Argon was set at 1.5 atm pressure for gold deposition on the sample surface. It is important to take into account that the deposition on both sides has to be coincident so that the electrodes remain parallel and the electric path is minimal.



Figure 14: Pieces of the pellets (Figure 13) after the deposition of the gold coating using a shadow mask.

3.2.5 XRD

A structural analysis of the precursors and the composites is made through X-ray diffraction measurements. The instrument used is a model Bruker D8-focus Advance with $\text{CuK}\alpha$ radiation, a LynxEye™ SuperSpeed Detector and a 90 position sample changer. The samples, as powders, are placed in a sample holder and flatten and smoothen their surface with a piece of thin glass. The parameters used are the standard for a crystalline experiment from 10 to 75 degrees 2θ , with a slit-opening of 0.2° .

The data was studied by the software tool DIFFRAC.SUITE TOPAS®, with necessary corrections and applying Rietveld refinement for every pattern obtained. The Rietveld refinement involved comparing crystallographical data from the precursors with the peaks from the experimental data obtained. For the composite, we used separately the structural data from the precursors phases "Amm2" and "Cmcm" for TMA FBC, and "P4mm" for BaTiO_3 . Finally, this software enables us to obtain the mass percentage of each phase.

3.2.6 SEM

The surface characterization of the samples, both the precursors and the composites of different compositions, is performed with a variable-pressure Scanning Electron Microscope. This instrument is a Hitachi Model S-3400N PC-based. It is used with automatic

brightness, contrast and focus control and the images are obtained at high voltage (around 10 kV). The scale varies in the different images and is specified in each of them.

3.2.7 Pycnometry

For the density evaluation of the samples, a gas pycnometer is used: the AccuPyc II 1340 Gas Displacement Pycnometry System of Micromeritics®. In this case, the analysis gas is Helium and 10 purges are conducted. The sample chamber used has 10 cm³.

3.2.8 PSD Analysis

For the particle size analysis of the BaTiO₃, a Laser Scattering Particle Size Distribution (PSD) Analyser is used. This is a Partica LA-960 instrument belonging to HORIBA, Ltd. Manufacturing Company. The analyser can measure particle sizes between 10 nanometres and 5 millimetres. During the analysis, the particles are dispersed in distilled water and the measures are made at 82.7 % of transmittance R and 81.9 % of transmittance B.

3.2.9 Ferroelectric measurements

The different composites undergo an electric analysis, by measuring ferroelectricity under High Voltage (up to 10 kV) with an AIXPES instrument. This modular system contains a TF analyser and a piezo sample holder unit. A Light Amplification by Stimulated Emission of Radiation (LASER) beam is used for the deflection of the samples during the measures. The samples are immersed in oil to enhance the flow of electric current. For this characterization process, it is applied a trapezoid-shaped electric field with time, as seen in Figure 15.

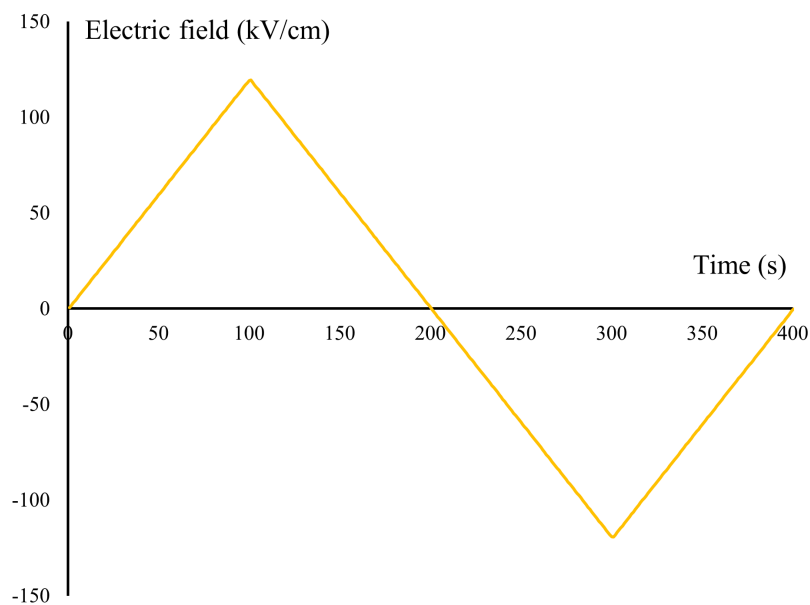


Figure 15: Graphic plot representing the applied Electric field vs. time, during the ferroelectric tests.

The data is collected with different hysteresis Amplitudes (V), as a function of the thickness of the samples, that is as integer multiples of their respective thickness. These are measured with a micrometre and represented in Table 4. The applied hysteresis frequency (Hz) is 10 Hz in the Polarization ($\mu\text{C}/\text{cm}^2$) and Strain (%) vs. Electric field (kV/cm) plots. The measures are also taken at different frequencies (1 Hz, 10 Hz and 100 Hz).

Table 4: Thickness measured for the hot-pressed pellets of the different compositions.

% in volume of ceramic	Thickness (mm)
10 %	0.31
30 %	0.38
50 %	0.58

3.2.10 Dielectric measurements

For dielectric impedance measurements, we also use a modular instrument. A Probo-Stat™ is employed as a sample holder, in a NORECS instrument and with a Trek Model 623B, as a High Voltage amplifier. The electrodes are connected to the sample holder in order to measure the dielectric constant and dielectric loss, with an applied frequency. The data is acquired at room temperature. The results collected consist of the dielectric constants (ϵ' and ϵ'') and the dielectric loss ($\tan(\delta)$). For this process, it is needed to know the size of the electrodes (diameter), formed by the deposition of gold, as mentioned before. This data is measured with a micrometre and recorded in Table 5.

Table 5: Diameter of the electrodes in the different bulk pellets used for the dielectric measurements.

% in volume of ceramic	Electrode diameter (mm)
10 %	3.19
30 %	3.12
50 %	3.35

4 Results

4.1 TMA FBC

After synthesizing the plastic crystal (TMA FBC), it is interesting to check its structural and surface features. For this purpose, the crystals are studied through different analytical techniques, such as X-ray diffraction and observed through Scanning Electron Microscope.

4.1.1 Structural Characterization

The synthetic TMA FBC is characterised structurally by X-ray diffraction analysis as a powder, so a mortar and a pestle are used for this purpose. With the data obtained, after performing the Rietveld refinement with the software tool already described, different phases are detected in the sample. These phases include "Amm2" and "Cmcm" (a secondary phase of the TMA FBC), among other unknown peak (marked in the plot). The appearance of unknown and secondary phases is an unwanted result for the following procedures, so better techniques may be required for the optimization of the synthesis. The resulting XRD plot treated with the software can be seen in Figure 16.

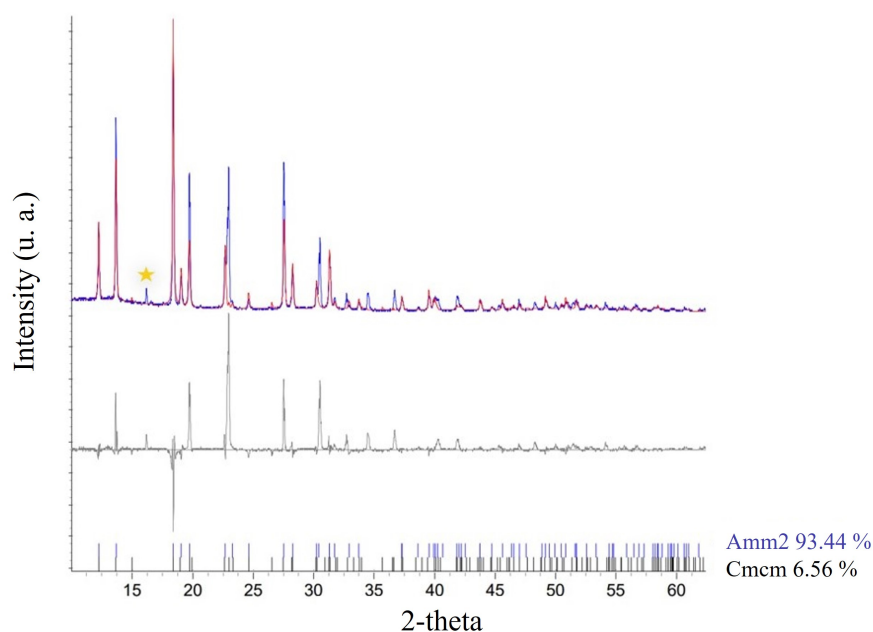


Figure 16: Plot of the Rietveld refinement results of the XRD pattern from the TMA FBC, including the powder diffraction pattern with the fit (top) and the difference pattern (middle), together with the peak positions of the fitted structures (bottom). An unknown peak is marked with a star.

4.1.2 Surface Characterization

The structure of the TMA FBC is observed with Scanning Electron Microscopy (SEM). It is analysed in the form of crystals, with dendritic growth shown in Figure 17. In this case, a grain size of $80\ \mu\text{m}$ is observed. The surface of the hot-pressed pellet at $250\ ^\circ\text{C}$, made only with the plastic crystal, was also analysed in Figure 18.

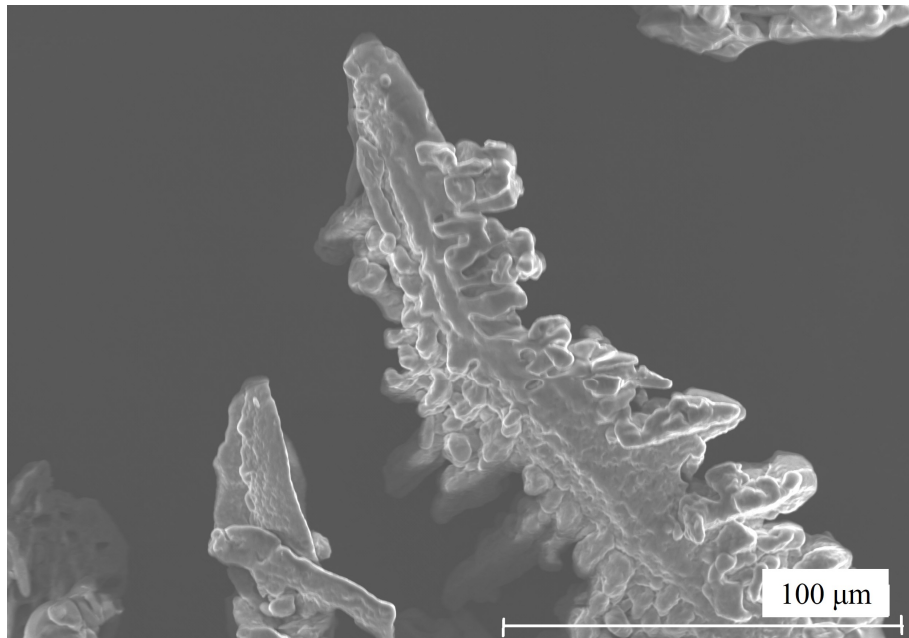


Figure 17: Plastic crystal dendrite observed with SEM, scale included.

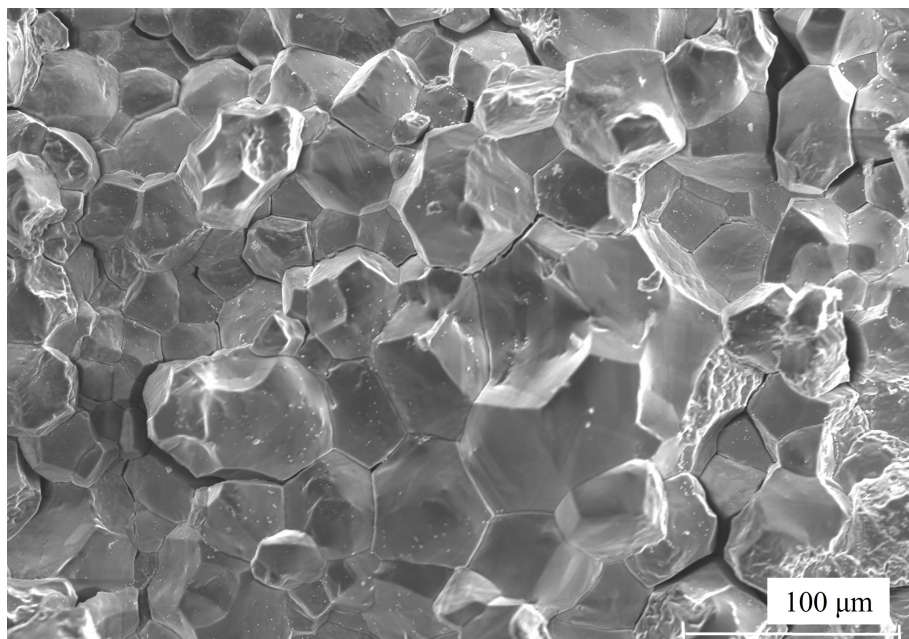


Figure 18: SEM image of a hot-pressed pellet fracture surface of the plastic crystal, scale included.

4.2 BaTiO₃

With the aim of checking the suitability of the commercial BaTiO₃ (Sigma Aldrich) available for the objective of the project, deep characterization of the powder is performed. Several instruments are used such as an X-ray diffraction analyser, a pycnometer, and a Particle Size Distribution analyser and also it is observed through the Scanning Electron Microscope.

4.2.1 Structural Characterization

Firstly, a structural characterization is performed through X-ray diffraction analysis of the raw powder (Figure 19). Another X-ray diffraction analysis (Figure 20) is made after drying the powder at 120 °C in a vacuum oven, for 5 hours.

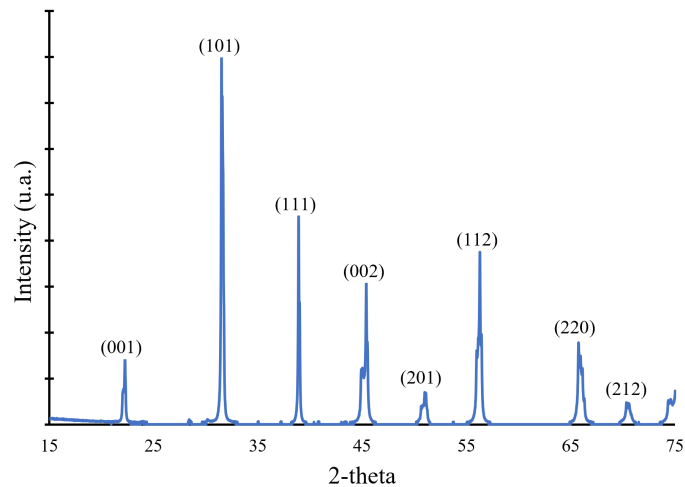


Figure 19: X-ray diffractogram of BaTiO₃ raw, before drying it with the vacuum oven, with the peaks labelled according to literature [20].

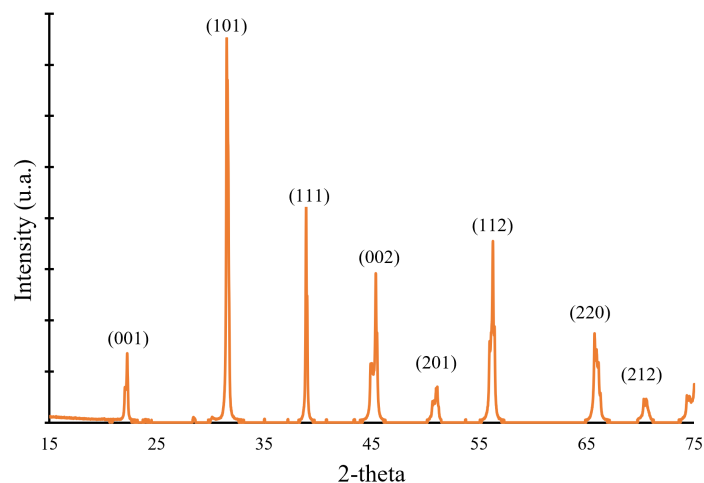


Figure 20: X-ray diffractogram of BaTiO₃ dried in the vacuum oven at 120 °C, with the peaks labelled according to literature [20].

4.2.2 Density Characterization

The density of the commercial BaTiO₃ is measured with a pycnometer, using the conditions already specified. It is observed that the experimental density of the powder available has a value of $6.139 \pm 0.023 \text{ g/cm}^3$. For this procedure, the volume of the ceramic measured had a value of $1.127 \pm 0.004 \text{ cm}^3$.

4.2.3 Particle-Size Distribution Characterization

In order to determine the particle size of the ceramic powder a Particle Size Distribution (PSD) analyser was used. The resulting distribution is shown in Figure 21. The average value is $3.224 \pm 0.0750 \text{ }\mu\text{m}$.

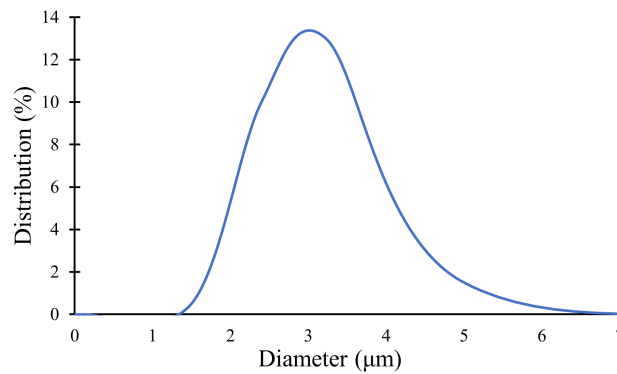


Figure 21: Graphic plot of the distribution of the particle sizes obtained through the PSD analysis of BaTiO₃ powder.

4.2.4 Surface Characterization

With the purpose of taking a deeper insight into the powder, it is also analysed through SEM images. In Figure 22, it can be checked that the grain size is less than $1 \text{ }\mu\text{m}$, which is inconsistent with the PSD analysis. With this data, we can predict that the grains of the powder are aggregated in clusters of over $3 \text{ }\mu\text{m}$, confirmed by the PSD analysis.

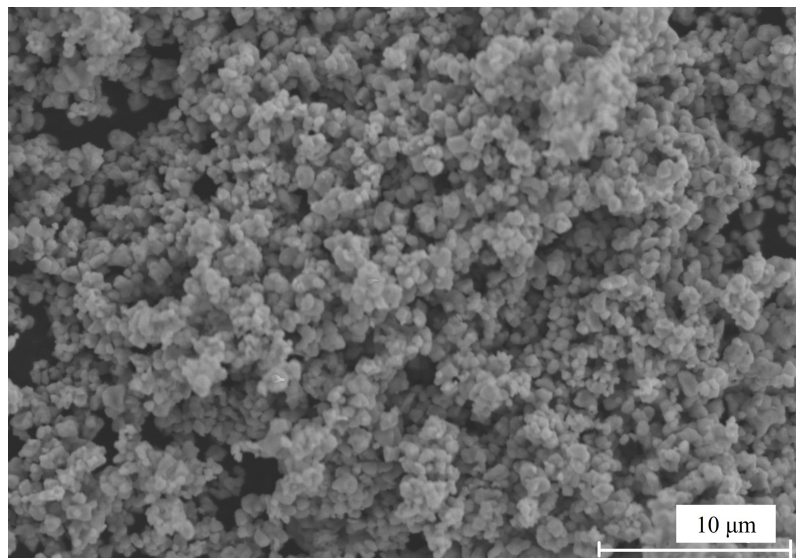


Figure 22: BaTiO₃ powder observed with SEM, scale included.

4.3 Composite

After mixing the plastic crystal and perovskite powders in different volume ratios, and obtaining the pellets with the hot press instrument, they can be characterised through different techniques, such as X-ray diffraction, observed through SEM images and finally, we can study their electrical properties. By comparing the different compositions, we can observe how the sought properties change.

4.3.1 Structural Characterization

Firstly, in the form of a mix of powders, before the press, the composites are analysed through X-ray diffraction, in Figures 23, 24 and 25. With this technique, after applying the software tools, it can be obtained the weight ratios of the different phases of the composites ("Amm2" and "Cmcm" for TMA FBC and "P4mm" for the BaTiO₃). In order to compare these ratios with the originals intended, we can use the density of both of the precursors. The volume ratios found in the samples are gathered in Table 6.

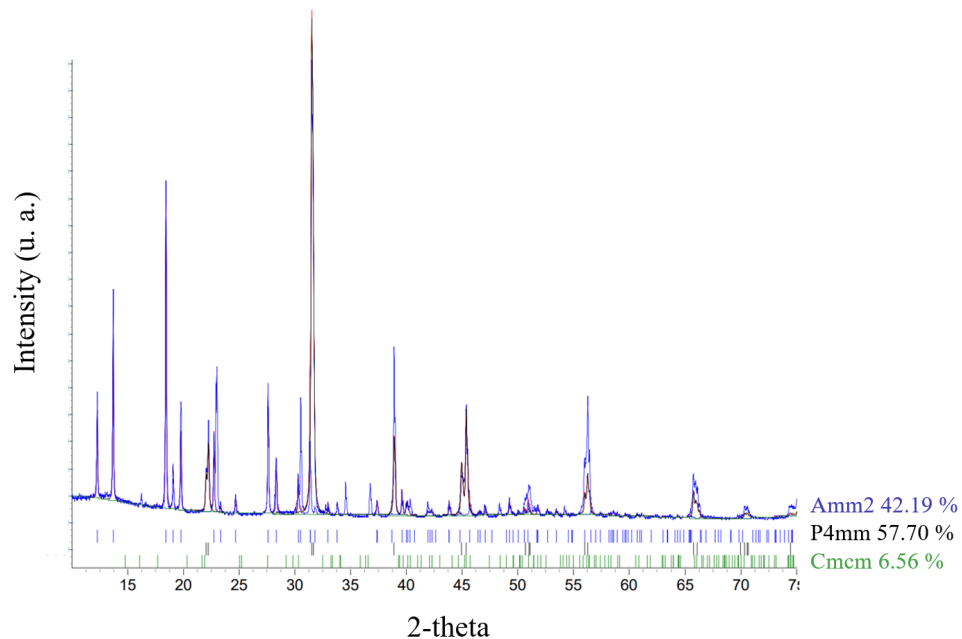


Figure 23: Plot of the Rietveld refinement results of the XRD pattern from the composite with 10 % of BaTiO₃ in volume, including the powder diffraction pattern and fit, together with the peak positions of the fitted structures.

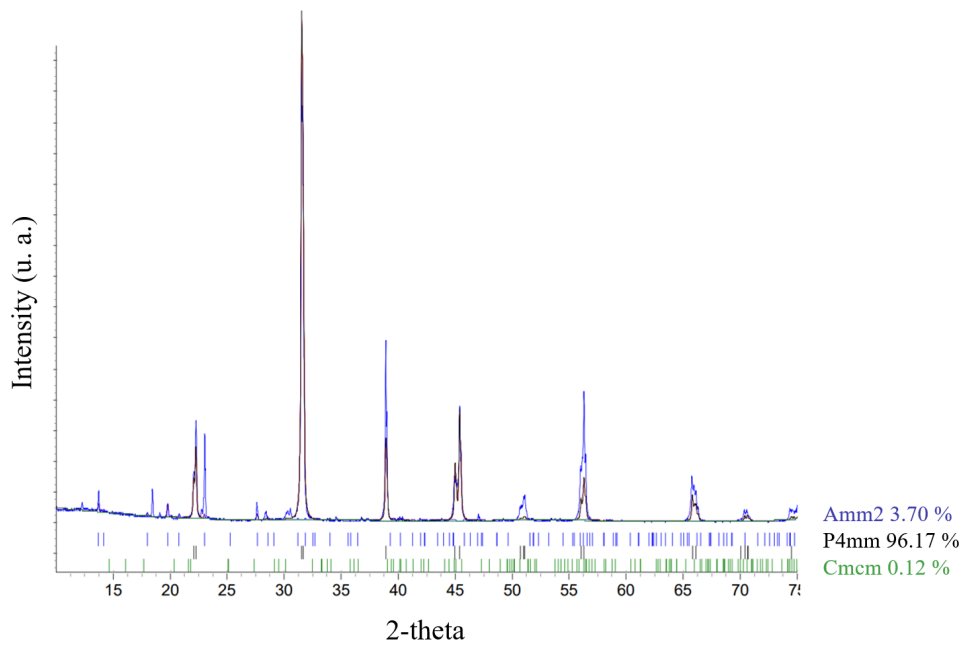


Figure 24: Plot of the Rietveld refinement results of the XRD pattern from the composite with 30 % of BaTiO₃ in volume, including the powder diffraction pattern and fit, together with the peak positions of the fitted structures.

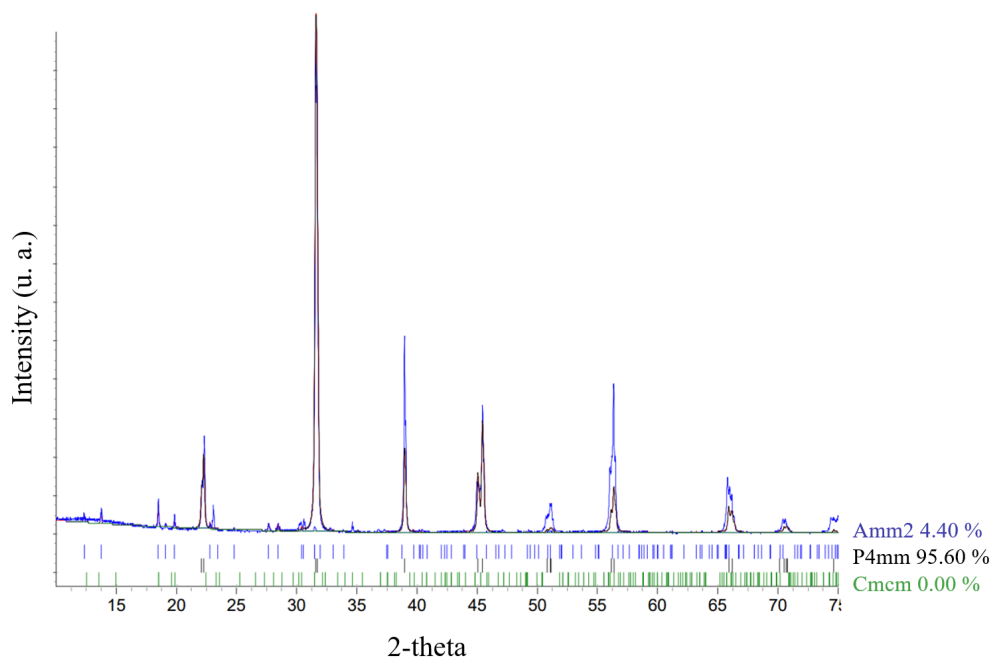


Figure 25: Plot of the Rietveld refinement results of the XRD pattern from the composite with 50 % of BaTiO₃ in volume, including the powder diffraction pattern and fit, together with the peak positions of the fitted structures.

Table 6: Experimental results and theoretical values of weight and volume % of BaTiO₃ in the different composites.

Experimental weight %	Experimental volume %	Theoretical volume %
57.7 %	24.8 %	10.0 %
96.2 %	85.9 %	30.0 %
95.6 %	84.0 %	50.0 %

4.3.2 Density Characterization

The densities of the different mixtures of powders (10, 30 and 50 % of BaTiO₃ in volume) are measured in the pycnometer. The obtained values are plotted into a graph in Figure 26, in which it is also represented the theoretical densities of the precursors of the composite. In this case, we can see a linear dependence between the density of the composite and the volume proportion of the ceramic in it, as expected.

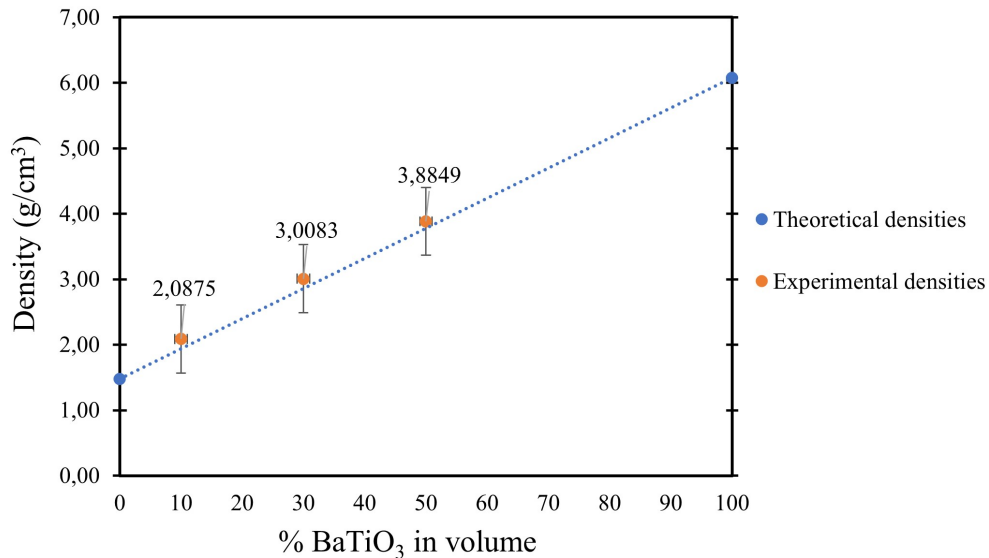


Figure 26: Graphic plot representing the experimental density values of the different proportions of BaTiO₃ and TMA FBC.

4.3.3 Surface Characterization

The hot-pressed pellets obtained are observed with the SEM, in order to determine the appearance and visual distribution of the plastic crystal and the ceramic. The resulting images are collected in Figures 27, 28, 29, 30, 31, 32, 33 and 34, identifying the sections that correspond to the different compounds in each case. Photographs of the surface of the pellets, as well as of the longitudinal face of the cuts, have been recorded.

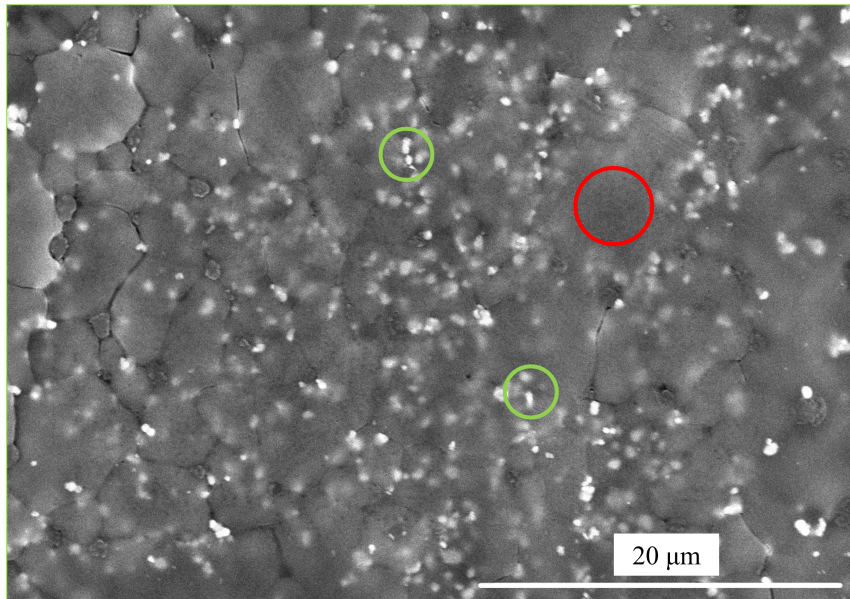


Figure 27: Surface of the composite with a 10 % ratio of BaTiO_3 , observed with SEM, scale included and parts identified (red for the TMA FBC and green for the BaTiO_3).

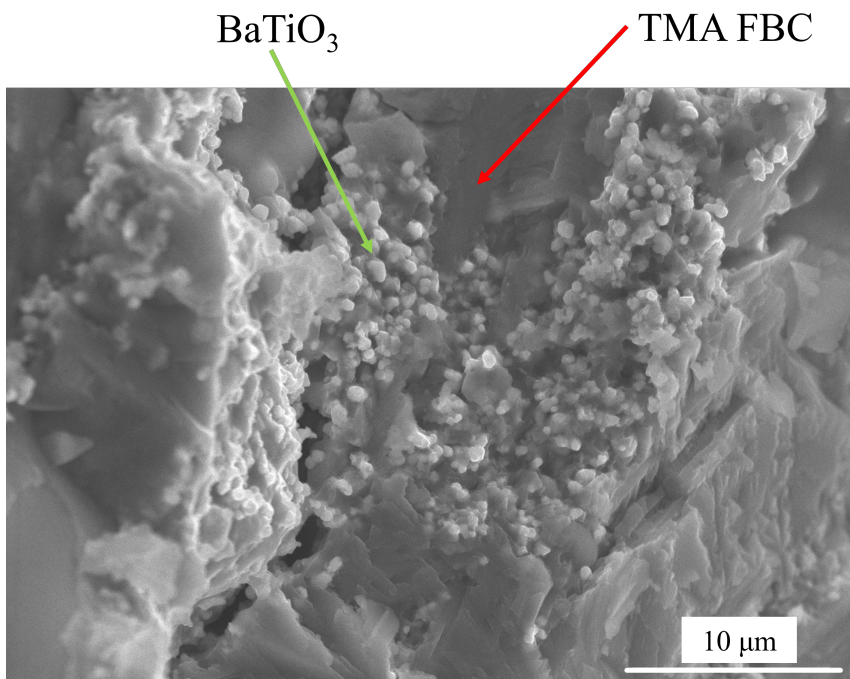


Figure 28: Longitudinal cut surface of the composite with a 10 % ratio of BaTiO_3 , observed with SEM, scale included and parts identified (red for the TMA FBC and green for the BaTiO_3).

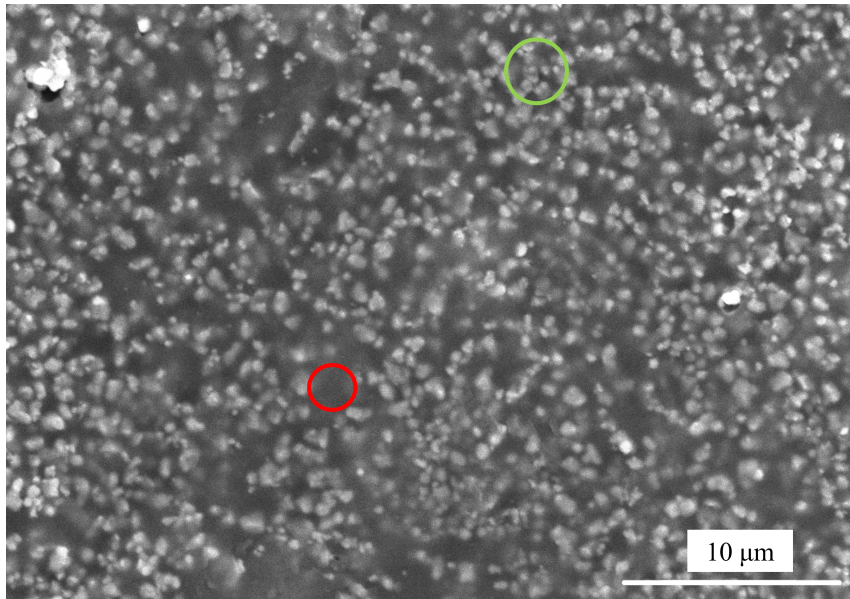


Figure 29: Surface of the composite with a 30 % ratio of BaTiO_3 , observed with SEM, scale included and parts identified (red for the TMA FBC and green for the BaTiO_3).

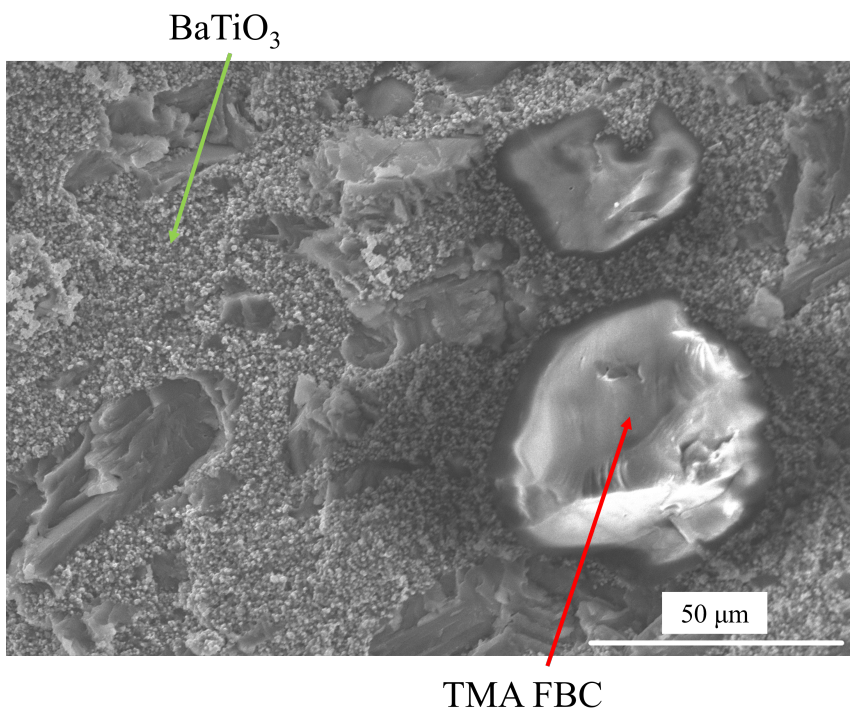


Figure 30: Longitudinal cut surface of the composite with a 30 % ratio of BaTiO_3 , observed with SEM, scale included and parts identified (red for the TMA FBC and green for the BaTiO_3).

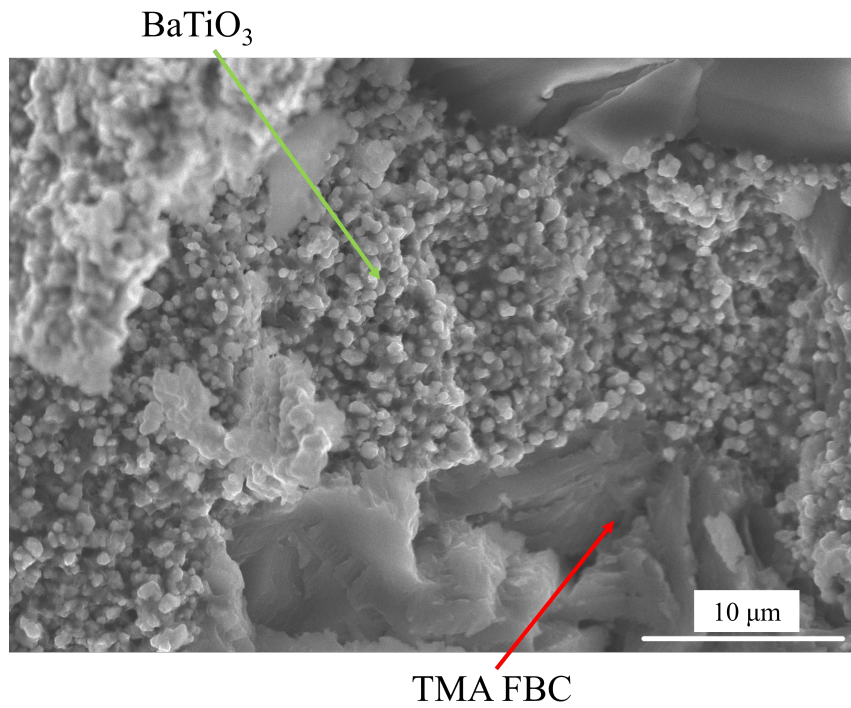


Figure 31: Closer longitudinal cut surface of the composite with a 30 % ratio of BaTiO₃, observed with SEM, scale included and parts identified (red for the TMA FBC and green for the BaTiO₃).

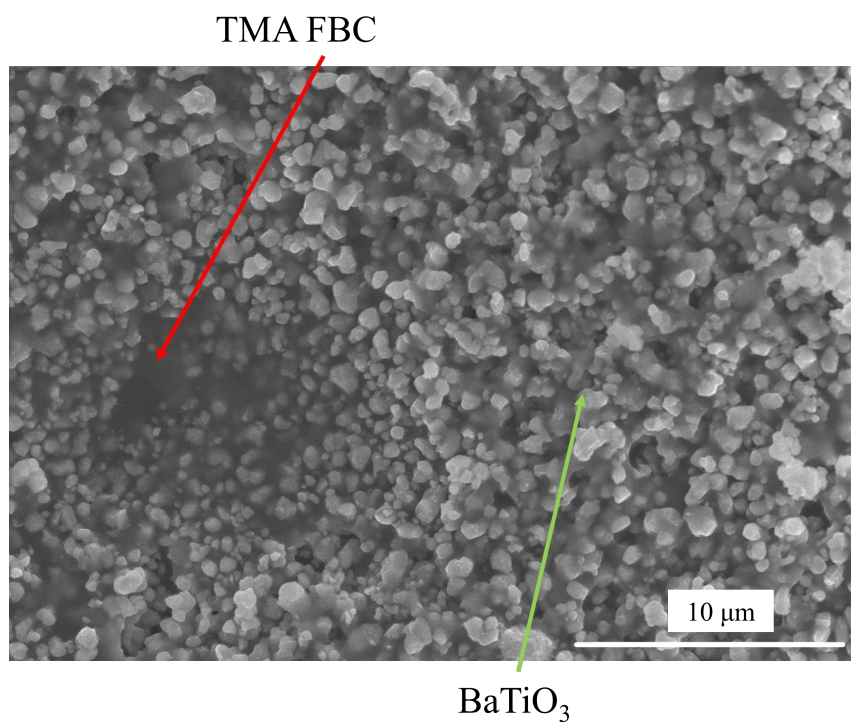


Figure 32: Surface of the composite with a 50 % ratio of BaTiO₃, observed with SEM, scale included and parts identified (red for the TMA FBC and green for the BaTiO₃).

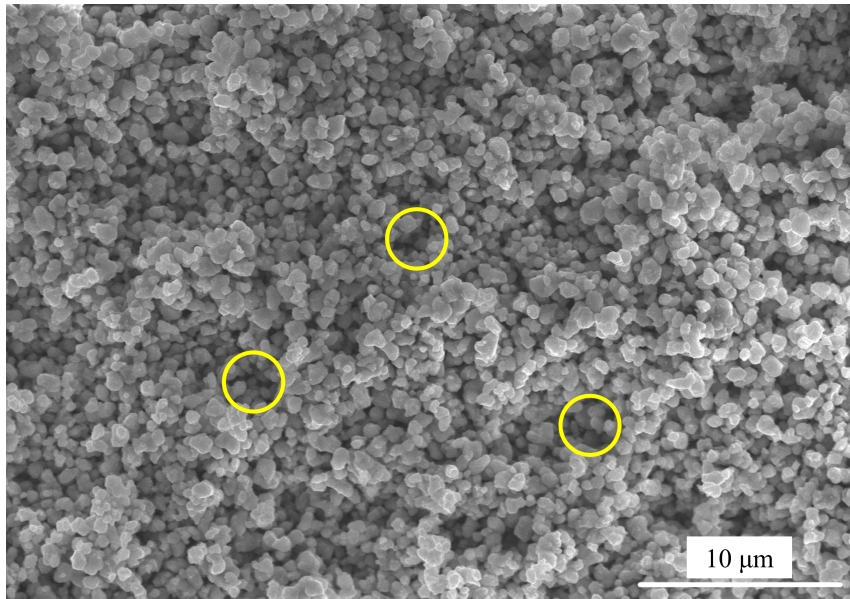


Figure 33: Surface of the composite with a 50 % ratio of BaTiO₃, observed with SEM, scale included with porosities marked in yellow.

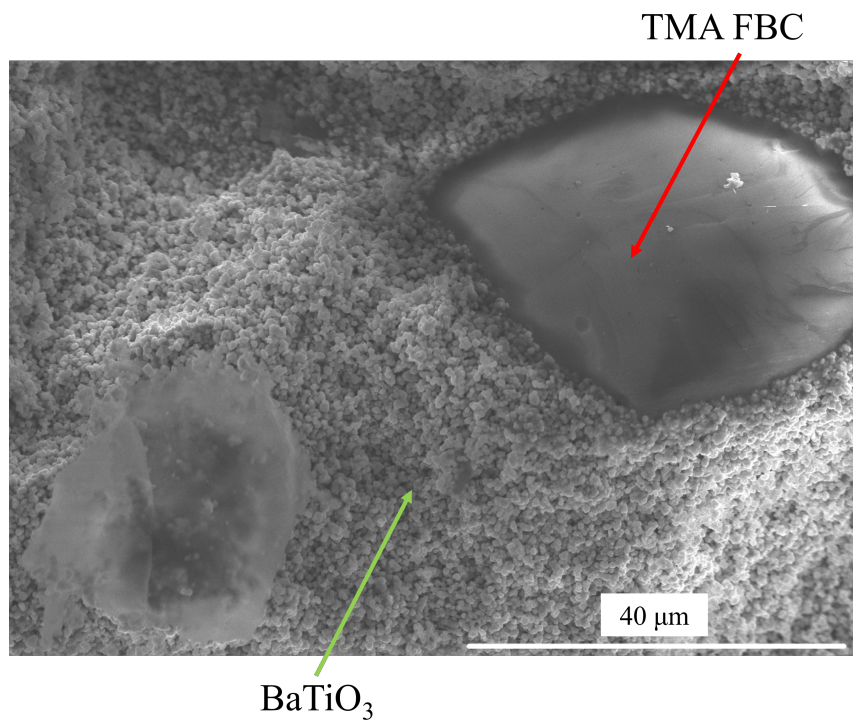


Figure 34: Longitudinal cut surface of the composite with a 50 % ratio of BaTiO₃, observed with SEM, scale included and parts identified (red for the TMA FBC and green for the BaTiO₃).

4.3.4 High Voltage Ferroelectric Properties Characterization

After using the gold sputter coater, the pellets are prepared for the electrical measurements, as they have suitable parallel electrodes on each of their surfaces. The relations

between the electric field applied and the polarization are represented in Figures 35, 36, 37 and 38, while the relation between the electric field applied and the strain of the samples are recorded in Figures 39, 40 and 41. The darker shades of colours represent higher applied hysteresis amplitude (V). As explained before, the hysteresis amplitude is calculated through integer multiples of the thickness of each sample. In the represented plots, only the highest amplitudes are registered, from 6-9 kV.

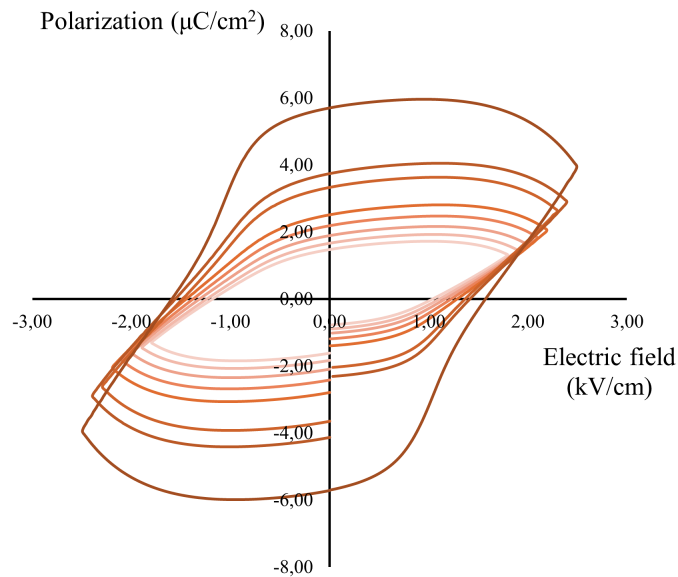


Figure 35: Ferroelectric test, Polarization vs Electric field loop of the 10 % of BaTiO₃ composite, measured at hysteresis frequency of 10 Hz.

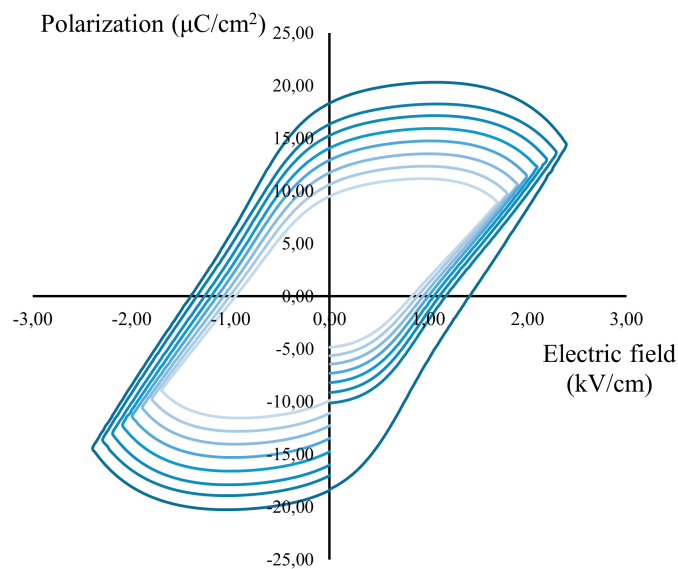


Figure 36: Ferroelectric test, Polarization vs Electric field loop of the 30 % of BaTiO₃ composite, measured at hysteresis frequency of 10 Hz.

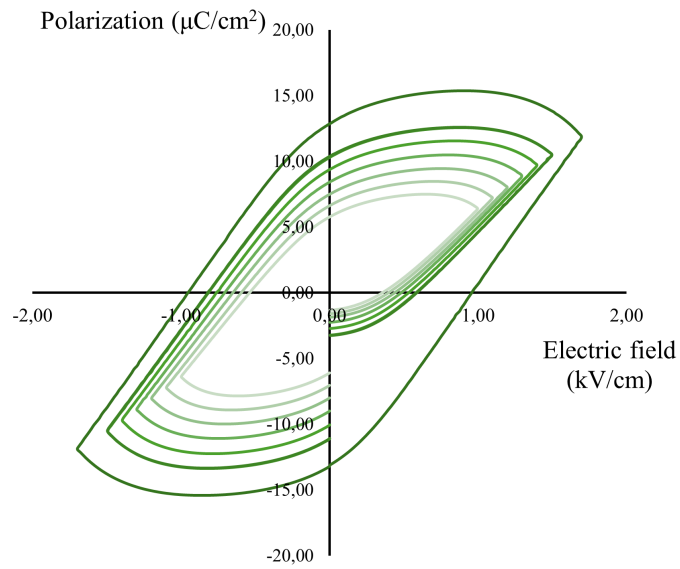


Figure 37: Ferroelectric test, Polarization vs Electric field loop of the 50 % of BaTiO₃ composite, measured at hysteresis frequency of 10 Hz.

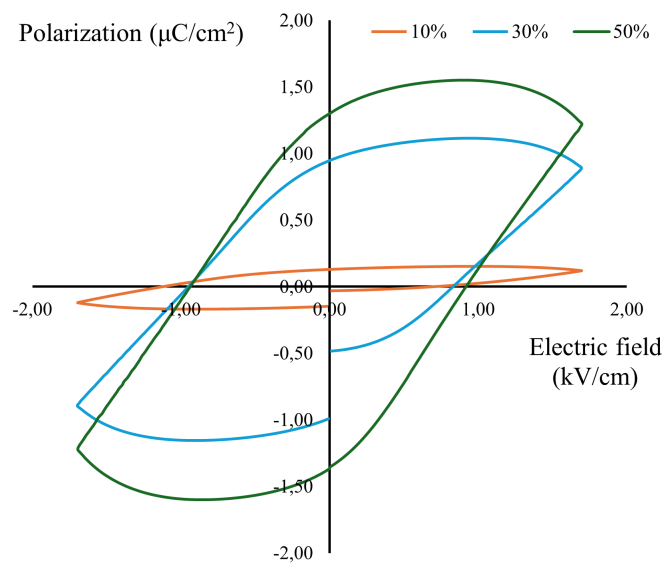


Figure 38: Ferroelectric test, Polarization vs Electric field loop of the composites, measured at the same hysteresis amplitude and hysteresis frequency of 10 Hz.

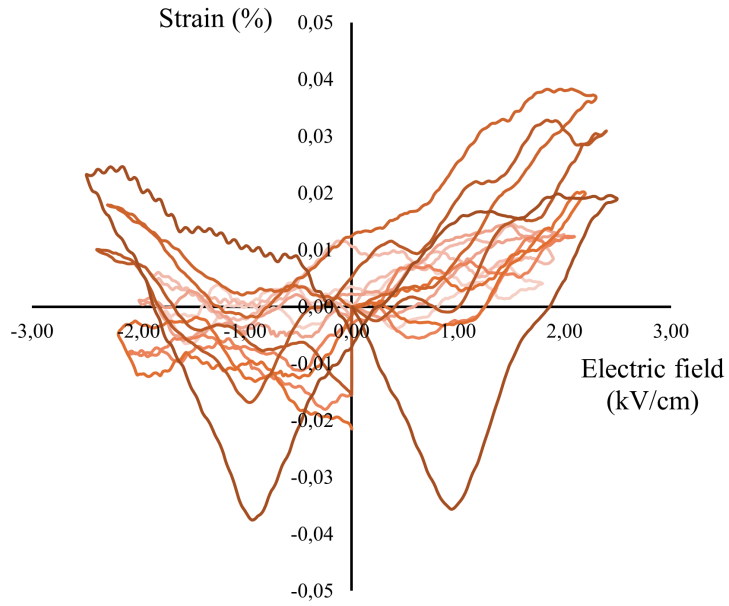


Figure 39: Ferroelectric test, Strain(%) vs Electric field graphic of the 10 % of BaTiO₃ pellet, measured at hysteresis frequency of 10 Hz.

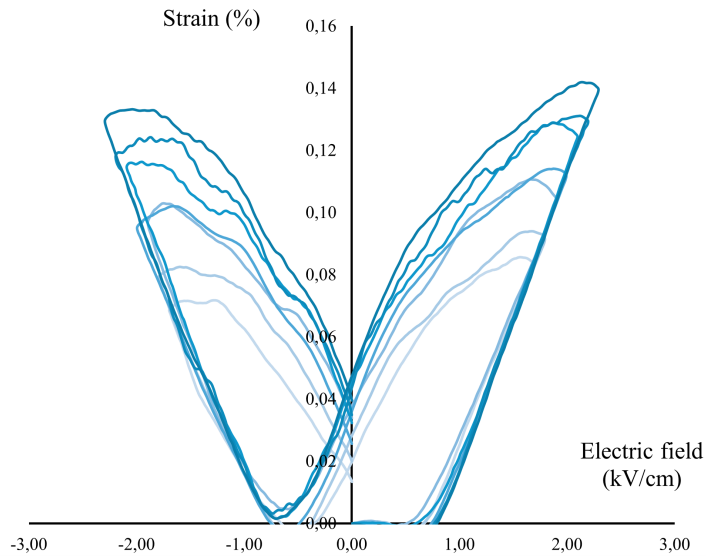


Figure 40: Ferroelectric test, Strain(%) vs Electric field graphic of the 30 % of BaTiO₃ pellet, measured at hysteresis frequency of 10 Hz.

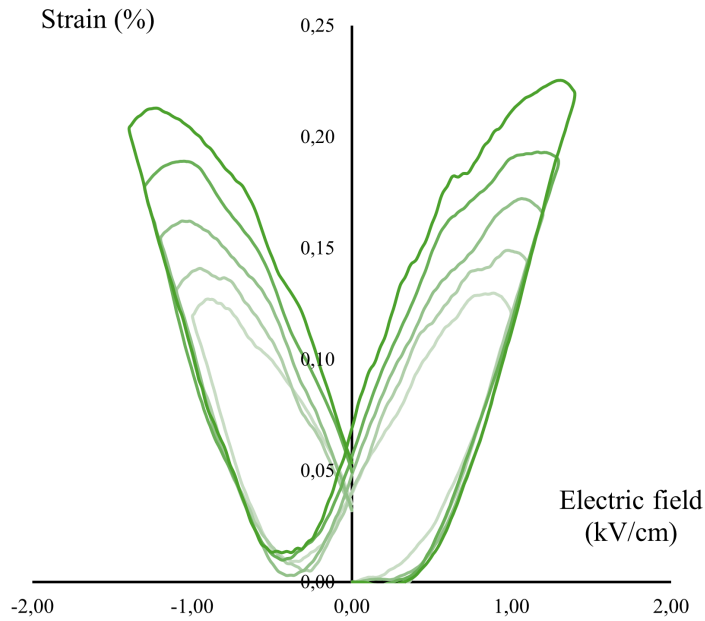


Figure 41: Ferroelectric test, Strain(%) vs Electric field graphic of the 50 % of BaTiO₃ pellet, measured at hysteresis frequency of 10 Hz.

4.3.5 Dielectric Properties Characterization

To have a deeper insight into the electric characteristics of the composites, with different compositions, a dielectric study of the samples is conducted. The dielectric instrument measures the dielectric constant and the loss through parameters like ϵ' , ϵ'' or $\tan(\delta)$, changing the frequency. These parameters can be related to each other with the following equation:

$$\tan(\delta) = \frac{\epsilon''}{\epsilon'}$$

It is interesting to plot the dielectric constant (ϵ') and the dielectric loss ($\tan(\delta)$) vs. the frequency and check the tendency with the changing composition, as shown in Figures 42 and 43, respectively.

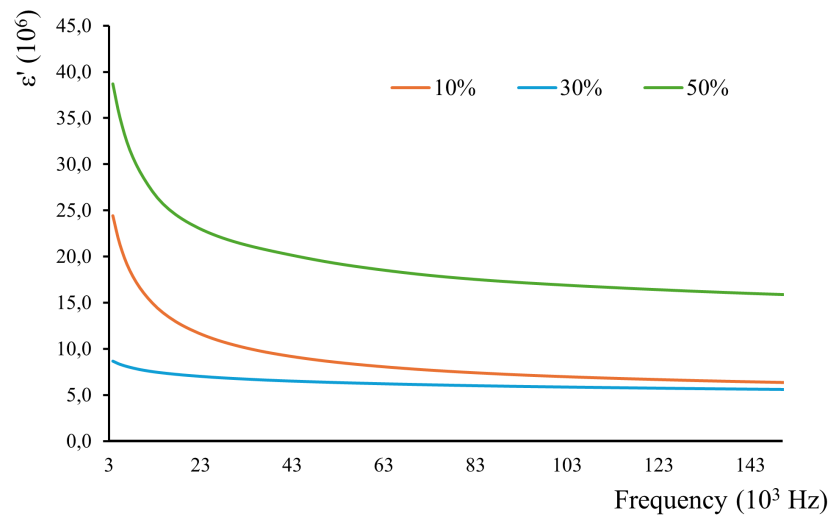


Figure 42: Graph representing the ϵ' vs frequency of the samples, represented with different colours.

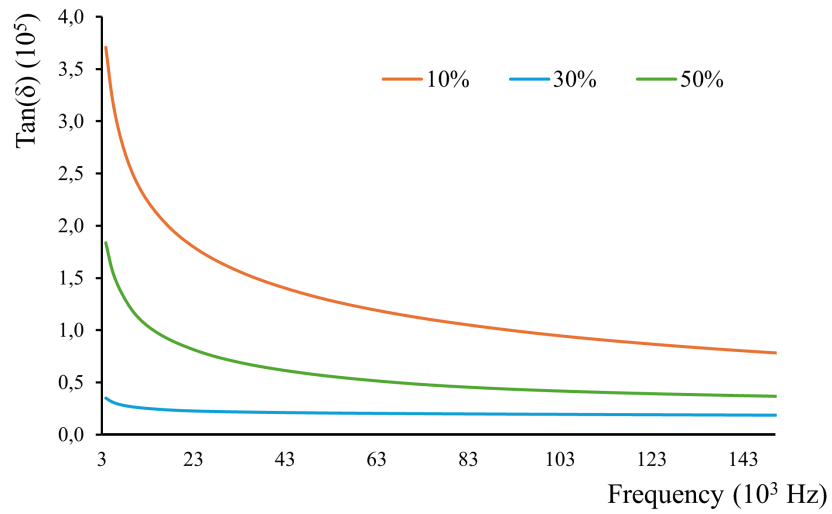


Figure 43: Graph representing the $\tan(\delta)$ vs frequency of the samples, represented with different colours.

5 Discussion

5.1 TMA FBC Synthesis and Characterization.

The TMA FBC was synthesized and characterized to determine its suitability, as the matrix of a new material for this project.

Firstly, through X-ray diffraction analysis, the presence of different phases in TMA FBC is observed. This is verified by comparing the X-ray diffraction spectra obtained (Figure 16) with the theoretical data of the "Amm2" and "Cmcm" phases of the plastic crystal. From the literature [15], we know that the studied phase with the best ferroelectric properties (larger hysteresis), and therefore the phase of interest, is "Amm2". The expected and sought phase "Amm2" predominated, however, the "Cmcm" phase was also found at 6.56 % by weight in the product. Additionally, in the pattern of the structural analysis, an unknown peak can also be seen, which is indicated by a star in the Figure.

A study of the surface is conducted through SEM image characterization. As expected, a dendritic growth is observed in the synthetic crystals, which are approximately 30 μm wide (Figure 17). On the other hand, when studying the image of the plastic crystal pellet, pressed at 250 °C, it is evident that the object exhibits a "ceramic" structure. This unexpected result may be due to the temperature at which the pellet was fabricated. During the process of pellet formation, the crystals were melted and restructured, as shown in Figure 18. A larger study will be necessary to comprehend the structural reorganization process of this compound.

5.2 Ceramic Characterization.

Through the characterization of BaTiO₃, as a commercial powder, it has been possible to verify its validity for the fabrication of the composite.

The X-ray diffraction analysis before (Figure 19) and after (Figure 20) drying the powder helped to conclude that the powder was suitable and dried. Using the mentioned software and comparing it with theoretical data, it was found that there was no discernible difference between the powder, before and after the drying process.

The ceramic density value (6.139 g/cm³) is acquired through pycnometer analysis. The value registered in the literature [12] of the theoretical density is 6.080 g/cm³, so the data obtained does not differ too much from the expected.

Additionally, the study of particle size was necessary, as the literature indicates a specific size is required for appropriate ferroelectric properties [9]. In the PSD analysis (Figure 21), it is observed that the BaTiO₃ particles have a consistent diameter size of around 3 μm . However, in the SEM image (Figure 22), it seems that the ceramic grains are smaller than this value (around 1 μm). Thus the particles appear to be strongly agglomerated with an average size of the clusters of 3 μm , comprising numerous smaller grains. Since the size can affect the piezoelectric and ferroelectric properties of the BaTiO₃ and its related materials, especially with grains smaller than 1 μm , we should be aware of possible effects. Therefore, future studies may need to involve annealing the material and promoting the growth of larger grains to avoid side effects.

5.3 Composites Characterization.

After obtaining the combined composites and performing their characterizations, several observations were made.

Firstly, in the preparation of the compounds, it was decided to fabricate them using different volume proportions of both precursors and then, use a hot press to obtain pellets, for easy study.

Fabricating these hot-pressed pellets, we have observed several things. Regarding the press temperature chosen, the first batch of pellets is pressed at 250 °C, but it resulted in burnt and not attached samples, that is why a new and final batch is made at 200 °C, with a successful result (Figure 13). While using the specified hot press, the pellets formed do not have an even density, especially at the edges. This is due to the lack of restriction on the horizontal flow of the composites. The final pellets end up being thin, on the order of hundreds of micrometres (Table 4) and fragile. However, they are still attached and homogenized enough to be processed and characterized (as seen in Figure 13). The difference in colour and tone through the pellets is also noticeable, being darker and more orange with a higher concentration of plastic crystal, a precursor that gives that characteristic colour. Also, a higher proportion of TMA FBC permits a better flow of the composite during the pellet formation, which allows for wider pellets.

Through the structural characterization with X-ray diffraction, the weight ratios of the phases in the samples have been determined, after applying the Rietveld refinement with the software. The weight ratios are described in each plot (Figures 23, 24 and 25), while the results of the conversion to volume ratios, in terms of the BaTiO₃, are presented in Table 6. These results are also compared with the theoretical volume % that is pursued. It is noticed that the experimental results exceed the expected values, especially for the composition of 30 % by volume of the ceramic. This discrepancy can be a consequence of the sum of the experimental error of the XRD analysis method and the precision in the treatment of the XRD data when using the said software, or the precision while taking a representative portion of the mix of the powders.

In the density study, the samples densities, obtained with the pycnometer measurements, have been compared with the theoretical data in Figure 26. In said graphical representation, the densities of the precursors are also shown, with a lineal tendency curve in the colour blue, that connects both values. The experimental density values, with their errors, fall within the tendency curve, so we can say that they present expected results, in terms of the different proportions. This gives evidence that the mix of powders is efficiently acquired, despite the results of the XRD analysis.

Several facts can be observed through the images recorded by SEM. By the remark of the previous SEM pictures, in Figures 18 and 22, it can be assigned the darkest areas in the composites to the TMA FBC appearance and the brightest and granulous areas to the BaTiO₃, as a way of differentiating the presence of both compounds in the samples. Firstly, in Figures 27 and 28, the 10 % composite is studied. As expected, a large area of TMA FBC is noticed (marked with a red circle and red arrow). Additionally, on the surface look, the TMA FBC exhibits a "ceramic" appearance. In this perspective, the presence of the ceramic (marked in green) seems to be low, while in the longitudinal

cut surface, it looks more abundant. This shows that the TMA FBC properties are still predominant, as it flows and restructures around the BaTiO₃ particles. Secondly, the 30 % composite, shown in Figures 29, 30 and 31, has a different appearance. It is evidenced that the proportion of BaTiO₃ is higher, as seen in the surface picture, while the areas of TMA FBC are less predominant and do not show the ceramic re-structuration. In the longitudinal surface cut, a large compacted grain of plastic crystal is observed inside the pellet, indicating the heterogeneity of the composite. The TMA FBC aggregates in areas without ceramic particles, marked with a red arrow. Finally, in Figures 32, 33 and 34, the 50 % in BaTiO₃ sample is characterized. In the surface look, the ceramic appeared to be prevailing, marked with the green arrow, but there are still some zones of continued TMA FBC matrix. In Figure 33, yellow circles have been used to mark some porosities found on the surface of the pellet. The porosities are not expected, due to the use of the hot press to fabricate the pellets. Also, their presence can unpredictably affect the electrical properties. This issue can be handled in a variety of methods: regarding the pellet preparation, we can use a new and more exhaustive grinding process, and during the press procedure, a higher temperature can be adjusted to reduce the TMA FBC viscosity, so its fluidity becomes better to enclose the pores. Ultimately, a different hot press, with a specific holder can be used, so the pellet becomes more dense and consistent. The longitudinal cut surface figure also presents some large areas of plastic crystal without the dispersion of the perovskite particles, as seen before in the previous sample.

Upon characterizing the material's electric properties, diverse outcomes were observed. For both, the ferroelectric and dielectric tests, the electric field used was applied to the samples through gold layer electrodes. As in the first measurements, the thickness of the samples are needed to be known, they are collected in Table 4. This is another visible feature of the variation in the concentration. When the proportion of BaTiO₃ is higher, the pellets seem to be thicker, so as the ceramic is denser and flows harder than the TMA FBC, more pressure would be needed to achieve the same thickness.

Regarding the ferroelectric tests, which are plotted in Figures 36 to 41, some observations can be made. These graphs show the ferroelectric hysteresis loops for the three materials with compositions of 10 %, 30 % and 50 % of BaTiO₃ by volume, measured at a frequency of 10 Hz. The observed loops show a clear ferroelectric behaviour, with a good symmetry around the origin, indicating a stable and reproducible ferroelectric behaviour, as well as low leakage. It is noticed that the polarization presents higher values, with a higher concentration of the ceramic. However, in the case of the 50 %, the effect is not observed because the hysteresis amplitudes are obtained with lower multiples of the pellet thickness. This sample is thicker, causing the equipment to reach almost the maximum of the possible applied voltage (10 kV). In Figure 38, the hysteresis loops of the three composites are collated in one plot. The ferroelectricity of the three pellets is measured with a hysteresis amplitude of 17000 times their respective thickness, so the data is equivalent. The remnant polarization, the coercive field and the saturation polarization are observed to increase with the ceramic content. Thus, for the concentration of 10 % (orange line), the remnant polarization and the coercivity are the lowest. While it increases for the others (30 %, blue line and 50 %, green line). As for the width of the hysteresis loop, it also increases in the same way as the previous parameters. The pellet with 50 % ceramic shows the widest loop. This indicates higher energy losses per hysteresis cycle

and a higher ferroelectric response. It is observed that, as the BaTiO₃ content increases, the material exhibits higher polarization capacity, coercivity, and loop width, indicating better ferroelectric properties. This is expected since the content of material with superior ferroelectric characteristics is higher. In Figures 39, 40 and 41, the relationship between the strain (in percentage) and the applied electric field has been represented for the three samples, respectively. This gives us information on how the material can be deformed with the application of the electric field. It can be observed that increasing the concentration of the ceramic in the pellets, significantly increases the percentage of strain. The pellet with 10 % BaTiO₃ shows a maximum strain of around ± 0.05 %, the one with 30 % shows a maximum of around ± 0.16 % and the pellet with 50 % BaTiO₃ exhibits a maximum strain of around ± 0.25 %. In addition, these curves show a non-linear behaviour typical of ferroelectric materials, and as the proportion of ceramic increases, the curve becomes more open, indicating greater losses in the material and a more significant response to changes in the electric field. This may suggest that pellets with higher BaTiO₃ concentrations can withstand higher electric fields without breaking since this ceramic is a material with a high deformation capacity in the presence of an electric field, which is consistent with its known ferroelectric properties.

Regarding the dielectric properties measured for the samples, whose results have been expressed in Figures 42 and 43, a series of conclusions have been reached. The first Figure represents the dielectric permittivity graph (ϵ'), in which it is observed that the dielectric permittivity of all the samples decreases asymptotically with increasing frequency. This is a typical behaviour in dielectric materials, due to the difficulty of the dipoles to align with the alternating electric field at high frequencies. On the other hand, it is observed that the dielectric permittivity decreases with the lower ceramic proportions. The sample with 50 % of BaTiO₃ in volume, has a significantly higher dielectric permittivity, which agrees with properties closer to ceramics, followed by the sample with 10 % and closely by the 30 % sample. The low dielectric permittivity observed in the 30 % ceramic sample, may be the result of a combination of particle scattering effects, interface interactions, matrix polarization or material compatibility. These factors may reduce the efficiency with which BaTiO₃ particles contribute to the dielectric permittivity of the composite, at this specific concentration. To better understand this behaviour, additional studies, such as simulation studies of the dielectric properties of the composite, would be useful. Finally, in the graph depicting the loss tangent ($\tan(\delta)$), in Figure 43, it can be observed that the relation between this parameter and the frequency is also asymptotically, for all compositions. This indicates that dielectric losses are higher at low frequencies and decrease at higher frequencies. The 10 % BaTiO₃ sample shows the highest loss tangent, followed by the 50 % sample, and finally the 30 % sample. Dielectric losses are influenced by both the matrix and the added material, and in this case, it appears that the optimal concentration for the lowest losses is 30 % of the ceramic, in volume.

6 Conclusions

The synthetic process for the plastic crystal, TMA FBC, has presented several challenges and observations. Firstly, the process is laborious, involving an essential recrystallization step to purify it and avoid the unwanted appearance of secondary phases. The presence of secondary phases has been observed during the structural characterization of the plastic crystal. However, it can be concluded that the synthesis was successful since the required phase constituted the majority (with 93.44 % by mass).

The characterization of the ceramic material has provided crucial information for its integration into the final composites. It has been learned that the different steps in the characterization involved numerous analyses, as well as comparing these with the literature. The particle size analysis revealed that the grains have a smaller size than preferred, but the particles agglomerate with an average of 3 μm of diameter. For the primary electrical applications and measurements of this project, this size seems sufficient. However, if the goal is to improve these features, it may be necessary to increase the size or consider using another source of BaTiO_3 .

In addition, the composite pellets, produced using hot pressing methods, were appropriate for the study of material properties. However, unexpected % weight (or volume) was observed in all of the samples through X-ray diffraction analysis. Performing this analysis was practical to obtain useful information about the compounds, as well as the use of SEM and other analytical instruments described. The depiction of these pellets, in terms of their ferroelectric and piezoelectric properties, provided a practical understanding of their primary electrical characteristics. It was observed that all the samples studied exhibited suitable ferroelectric behaviour, as evidenced by the hysteresis loops and strain representations, with varying values, as a function of the compositions, between 0.05 and 0.25 %. Additionally, they also present differences in their dielectric parameters, according to the different proportions of the plastic crystal and the ceramic, as well as with the changing frequency. Based on these results, it can be concluded that an intermediate concentration of BaTiO_3 (30 % in volume) in a material appears to minimize dielectric losses compared to lower (10 %) or higher (50 %) concentrations, although exhibiting lower dielectric permittivity at the same time. These findings could be beneficial for designing materials with specific dielectric properties, depending on the applications and desired operating frequencies.

In conclusion, we can say that this project has achieved its main objectives and has also opened up other paths for further work. Moreover, it has allowed us to build upon the new information, as well as apply the knowledge acquired in certain Chemistry Degree courses, such as "Química de Materiales" and "Química Inorgánica I, II, III".

References

- [1] Topolov V. Yu. and Bowen C. R. *Electromechanical Properties in Composites Based on Ferroelectrics*. Springer, 2009. ISBN: 978-1-84882-000-5.
- [2] Xu Y. *Ferroelectric Materials and their Applications*. North-Holland, 1991. ISBN: 978-0444883544.
- [3] Haertling G. H. “Ferroelectric Ceramics: History and Technology”. In: *J. Am. Ceram. Soc.* 82 (1999), pp. 797–818. DOI: 10.1111/j.1151-2916.1999.tb01840.x.
- [4] Walker J. et al. “Super-coercive electric field hysteresis in ferroelectric plastic crystal tetramethylammonium bromotrichloroferrate(III)”. In: *J. Mater. Chem. C* 8 (2020), p. 3206. DOI: 10.1039/C9TC06918F.
- [5] Corral-Flores V. and Bueno-Baqués D. “Flexible Ferroelectric BaTiO₃ – PVDF Nanocomposites”. In: *Ferroelectrics*. Ed. by Mickaël Lallart. Rijeka: IntechOpen, 2011. Chap. 17. DOI: 10.5772/16399.
- [6] *Ensure sustainable consumption and production patterns*. URL: <https://sdgs.un.org/goals/goal12> (visited on June 20, 2024).
- [7] Huang H. and Scott J. F. *Ferroelectric Materials for Energy Applications*. Wiley, 2018. ISBN: 9783527807475.
- [8] Whatmore R. “Ferroelectric Materials”. In: *Springer Handbook of Electronic and Photonic Materials*. Cham: Springer International Publishing, 2017, pp. 589–599. ISBN: 978-3-319-48933-9. DOI: 10.1007/978-3-319-48933-9_26.
- [9] Safari A., Panda R. K., and Janas V. F. “Ferroelectricity: Materials, Characteristics and Applications”. In: *Advanced Ceramic Materials*. Vol. 122. Key Engineering Materials. Trans Tech Publications Ltd, Sept. 1996, pp. 35–70. DOI: 10.4028/www.scientific.net/KEM.122-124.35.
- [10] Patri S. *Dielectric Materials: Introduction, Research and Applications*. 2009. ISBN: 978-1-60741-039-3.
- [11] Habib M., Lantgios I., and Hornbostel K. “A review of ceramic, polymer and composite piezoelectric materials”. In: *Journal of Physics D: Applied Physics* 55.42 (Aug. 2022), p. 423002. DOI: 10.1088/1361-6463/ac8687.
- [12] Acosta M. et al. “BaTiO₃-based piezoelectrics: Fundamentals, current status, and perspectives”. In: *Applied Physics Reviews* 4.4 (Dec. 2017), p. 041305. DOI: 10.1063/1.4990046.
- [13] Atikur Rahman M. et al. “Tailoring the Properties of Bulk BaTiO₃ Based Perovskites by Heteroatom-Doping towards Multifunctional Applications: A Review”. In: *ECS Journal of Solid State Science and Technology* 12 (Oct. 2023). DOI: 10.1149/2162-8777/ad00da.
- [14] Das S., Mondal A., and Reddy C. M. “Harnessing molecular rotations in plastic crystals: a holistic view for crystal engineering of adaptive soft materials”. In: *Chem. Soc. Rev.* 49 (24 2020), pp. 8878–8896. DOI: 10.1039/D0CS00475H.
- [15] Walker J. et al. “Mesophase Transitions in [(C₂H₅)₄N][FeBrCl₃] and [(CH₃)₄N][FeBrCl₃] Ferroic Plastic Crystals”. In: *Chemistry of Materials* 34.6 (2022), pp. 2585–2598. DOI: 10.1021/acs.chemmater.1c03778.
- [16] Shalaev E. et al. “Crystalline mesophases: Structure, mobility, and pharmaceutical properties”. In: *Advanced Drug Delivery Reviews* 100 (2016). Amorphous phar-

- maceutical solids, pp. 194–211. ISSN: 0169-409X. DOI: 10.1016/j.addr.2016.04.002.
- [17] Walker J. et al. “Electric field dependent polarization switching of tetramethylammonium bromotrichloroferrate(III) ferroelectric plastic crystals”. In: *Applied Physics Letters* 116.24 (June 2020), p. 242902. DOI: 10.1063/5.0004387.
- [18] Harada J. et al. “Ferroelectricity and Piezoelectricity in Free-Standing Polycrystalline Films of Plastic Crystals”. In: *Journal of the American Chemical Society* 140.1 (2018), pp. 346–354. DOI: 10.1021/jacs.7b10539.
- [19] Dash S. et al. “Ferroelectric ceramic dispersion to enhance the beta phase of polymer for improving dielectric and ferroelectric properties of the composites”. In: *Polym. Bull.* 78 (2021), pp. 5317–5336. DOI: 10.1007/s00289-020-03372-4.
- [20] Al-Shakarchi E. K. and Mahmood N. B. “Three techniques used to produce BaTiO₃ fine powder”. In: *SCIRP* 2 (2011), p. 11. DOI: 10.4236/jmp.2011.211175.

List of Figures

1	Venn diagram with the relations between electric properties of materials [8].	2
2	Typical hysteresis loop of the P vs E of a ferroelectric crystal [9].	3
3	Scheme on the relevant aspects of new ferroelectric materials.	4
4	Structural model of the unit cell of the face-centred cubic system BaTiO ₃ .	5
5	Temperature dependence of the relative dielectric constant of pure BaTiO ₃ [13].	6
6	Structural model of the unit cell of orthorhombic TMA FBC.	8
7	Scheme of the combined properties of a ceramic and a polymer composite [11].	8
8	Photograph of a filtering flask, funnel, filtering paper and the dark red crystalline product.	12
9	Photograph of the rotary evaporator used for the recrystallization, with its parts labelled.	12
10	Dark red TMA FBC crystals before (left) and after (right) the recrystallization process.	13
11	Mix of the composites in powder form, in a mortar and pestle.	13
12	Hot Press Model used for obtaining the composite pellets.	14
13	Pellets of 10, 30 and 50 % of BaTiO ₃ in volume from left to right, obtained with the flat heating hot press (diameters around 2-3 cm).	14
14	Pieces of the pellets (Figure 13) after the deposition of the gold coating using a shadow mask.	15
15	Graphic plot representing the applied Electric field vs. time, during the ferroelectric tests.	16
16	Plot of the Rietveld refinement results of the XRD pattern from the TMA FBC, including the powder diffraction pattern with the fit (top) and the difference pattern (middle), together with the peak positions of the fitted structures (bottom). An unknown peak is marked with a star.	18
17	Plastic crystal dendrite observed with SEM, scale included.	19
18	SEM image of a hot-pressed pellet fracture surface of the plastic crystal, scale included.	19
19	X-ray diffractogram of BaTiO ₃ raw, before drying it with the vacuum oven, with the peaks labelled according to literature [20].	20
20	X-ray diffractogram of BaTiO ₃ dried in the vacuum oven at 120 °C, with the peaks labelled according to literature [20].	20
21	Graphic plot of the distribution of the particle sizes obtained through the PSD analysis of BaTiO ₃ powder.	21
22	BaTiO ₃ powder observed with SEM, scale included.	21
23	Plot of the Rietveld refinement results of the XRD pattern from the composite with 10 % of BaTiO ₃ in volume, including the powder diffraction pattern and fit, together with the peak positions of the fitted structures. . .	22
24	Plot of the Rietveld refinement results of the XRD pattern from the composite with 30 % of BaTiO ₃ in volume, including the powder diffraction pattern and fit, together with the peak positions of the fitted structures. . .	23

25	Plot of the Rietveld refinement results of the XRD pattern from the composite with 50 % of BaTiO ₃ in volume, including the powder diffraction pattern and fit, together with the peak positions of the fitted structures. . .	23
26	Graphic plot representing the experimental density values of the different proportions of BaTiO ₃ and TMA FBC.	24
27	Surface of the composite with a 10 % ratio of BaTiO ₃ , observed with SEM, scale included and parts identified (red for the TMA FBC and green for the BaTiO ₃).	25
28	Longitudinal cut surface of the composite with a 10 % ratio of BaTiO ₃ , observed with SEM, scale included and parts identified (red for the TMA FBC and green for the BaTiO ₃).	25
29	Surface of the composite with a 30 % ratio of BaTiO ₃ , observed with SEM, scale included and parts identified (red for the TMA FBC and green for the BaTiO ₃).	26
30	Longitudinal cut surface of the composite with a 30 % ratio of BaTiO ₃ , observed with SEM, scale included and parts identified (red for the TMA FBC and green for the BaTiO ₃).	26
31	Closer longitudinal cut surface of the composite with a 30 % ratio of BaTiO ₃ , observed with SEM, scale included and parts identified (red for the TMA FBC and green for the BaTiO ₃).	27
32	Surface of the composite with a 50 % ratio of BaTiO ₃ , observed with SEM, scale included and parts identified (red for the TMA FBC and green for the BaTiO ₃).	27
33	Surface of the composite with a 50 % ratio of BaTiO ₃ , observed with SEM, scale included with porosities marked in yellow.	28
34	Longitudinal cut surface of the composite with a 50 % ratio of BaTiO ₃ , observed with SEM, scale included and parts identified (red for the TMA FBC and green for the BaTiO ₃).	28
35	Ferroelectric test, Polarization vs Electric field loop of the 10 % of BaTiO ₃ composite, measured at hysteresis frequency of 10 Hz.	29
36	Ferroelectric test, Polarization vs Electric field loop of the 30 % of BaTiO ₃ composite, measured at hysteresis frequency of 10 Hz.	29
37	Ferroelectric test, Polarization vs Electric field loop of the 50 % of BaTiO ₃ composite, measured at hysteresis frequency of 10 Hz.	30
38	Ferroelectric test, Polarization vs Electric field loop of the composites, measured at the same hysteresis amplitude and hysteresis frequency of 10 Hz.	30
39	Ferroelectric test, Strain(%) vs Electric field graphic of the 10 % of BaTiO ₃ pellet, measured at hysteresis frequency of 10 Hz.	31
40	Ferroelectric test, Strain(%) vs Electric field graphic of the 30 % of BaTiO ₃ pellet, measured at hysteresis frequency of 10 Hz.	31
41	Ferroelectric test, Strain(%) vs Electric field graphic of the 50 % of BaTiO ₃ pellet, measured at hysteresis frequency of 10 Hz.	32
42	Graph representing the ϵ' vs frequency of the samples, represented with different colours.	33

43	Graph representing the $\tan(\delta)$ vs frequency of the samples, represented with different colours.	33
----	--	----

List of Tables

1	Commercial compounds with their CAS used for the experimental procedures.	11
2	Stoichiometric relations and compounds used for the synthesis of 20 g of TMA FBC.	11
3	Amount of mass needed of the precursors to obtain the different composites.	14
4	Thickness measured for the hot-pressed pellets of the different compositions.	17
5	Diameter of the electrodes in the different bulk pellets used for the dielectric measurements.	17
6	Experimental results and theoretical values of weight and volume % of BaTiO ₃ in the different composites.	24